UNIVERSIDADE FEDERAL DE SANTA MARIA
CENTRO DE TECNOLOGIA
PROGRAMA DE PÓS-GRADUAÇÃO EM ENGENHARIA DE PROCESSOS

SÍNTESE DE FERRITA DE ZINCO ($ZnFe_2O_4$) POR DIFERENTES ROTAS E SEU USO NA REAÇÃO HETEROGÊNEA DE FOTO-FENTON

DISSERTAÇÃO DE MESTRADO

Chayene Gonçalves Anchieta

Santa Maria, RS, Brasil
2015

SÍNTESE DE FERRITA DE ZINCO ($ZnFe_2O_4$) POR DIFERENTES ROTAS E SEU USO NA REAÇÃO HETEROGÊNEA DE FOTO-FENTON

Chayene Gonçalves Anchieta

Dissertação apresentada ao Curso de Mestrado do Programa de Pós-Graduação em Engenharia de Processos, Área de Concentração em Desenvolvimento de Processos Agroindustriais e Ambientais, da Universidade Federal de Santa Maria (UFSM, RS), como requisito principal para obtenção do grau de **Mestre em Engenharia de Processos.**

Orientador: Prof. Dr. Edson Luiz Foletto

Santa Maria, RS, Brasil
2015

UNIVERSIDADE FEDERAL DE SANTA MARIA
CENTRO DE TECNOLOGIA
PROGRAMA DE PÓS-GRADUAÇÃO EM ENGENHARIA DE PROCESSOS

A Comissão Examinadora, abaixo assinada, aprova a Dissertação de Mestrado

SÍNTESE DE FERRITA DE ZINCO ($ZnFe_2O_4$) POR DIFERENTES ROTAS E SEU USO NA REAÇÃO HETEROGÊNEA DE FOTO-FENTON

Elaborada por
Chayene Gonçalves Anchieta

Como requisito parcial para obtenção do grau de
Mestre em Engenharia de Processos

COMISSÃO EXAMINADORA:

Prof. Edson Luiz Foletto, Dr. (UFSM)
(Presidente/Orientador)

Prof. Adriano Cancelier, Dr. (UFSM)

Prof. Osvaldo Chiavone-Filho, Dr. (UFRN)

Santa Maria, 2015

AGRADECIMENTOS

Primeiramente a Deus, por me iluminar nas escolhas dos melhores caminhos e pela proteção.
A minha família em especial meus pais, Olga e Luiz Carlos, e minha irmã Mylena, pelo amor incondicional, pelo apoio e incentivo para que eu continuasse em busca de meus objetivos.
Aos amigos Leonardo e Mariele que juntamente com minha mãe e irmã estiveram sempre ao meu lado, pela compreensão nos momentos de estresse e ausência.
Ao Nicholas pelas horas de estudo e paciência ao longo dessa trajetória acadêmica, onde junto com a Camila e a Juliana foram mais do que colegas, foram amigos que contribuíram muito para a concretização desse trabalho.
Ao Paulo R. Salbego pelo auxílio com as caracterizações do material e aos demais colegas do mestrado pelo tempo de convívio.
Ao Prof. Dr. Edson Luiz Foletto pela oportunidade de desenvolvimento deste trabalho, pela orientação, confiança e paciência nas correções do trabalho e em responder todos os e-mails.
Ao Prof. Dr. Marcio Antonio Mazutti pelas parcerias dentro da pesquisa e pelo auxílio com relação a infraestrutura.
Ao Prof. Dr. Erico M. M. Flores e o Edson I. Muller por contribuir com a síntese das amostras no microondas e ao Andre Gundel pelas análises de microscopia de força atômica realizadas na UNIPAMPA.
À Profª.Drª. Raquel C. Kuhn, ao Prof. Dr. Guilherme Luiz Dotto, ao Prof. Dr. Adriano Cancelier e ao Prof. Dr. Osvaldo Chiavone-Filho da UFRN, pelas contribuições nos artigos.
Às alunas de iniciação científica Luane Tochetto, Cristina Serpa, Heloisa Madalosso e Renata Sulkovski pela ajuda.
À Química Mariana Moro Bassaco do DEQ/UFSM, pelo apoio na realização das análises.
Ao André Friderichs e ao Departamento de Solos da Agronomia da UFSM pelo apoio nas análises de TOC no LabCeN: Laboratório de Pesquisa em Biotransformações de Carbono e Nitrogênio.
Ao Programa de pós-graduação em Engenharia de Processos da UFSM e aos demais professores e funcionários que contribuíram direta e indiretamente para minha pós-graduação.
À CNPq pelo incentivo financeiro.

RESUMO

Dissertação de Mestrado
Programa de Pós-Graduação em Engenharia de Processos
Universidade Federal de Santa Maria

SÍNTESE DE FERRITA DE ZINCO ($ZnFe_2O_4$) POR DIFERENTES ROTAS E SEU USO NA REAÇÃO HETEROGÊNEA DE FOTO-FENTON.

AUTORA: CHAYENE GONÇALVES ANCHIETA
ORIENTADOR: EDSON LUIZ FOLETTO
Data e Local da Defesa: Santa Maria, 20 de fevereiro de 2015.

Neste trabalho, foi realizada a síntese do óxido ferrita de zinco ($ZnFe_2O_4$) pelo método solvotérmico convencional e pela rota solvotérmica assistida por microondas. A influência das diferentes rotas de síntese, bem como de suas variáveis de síntese sobre as propriedades físicas do material foi investigada. Os pós obtidos foram caracterizados por difração de raios-X (DRX), espectroscopia no infravermelho (FTIR), medições de adsorção-dessorção de nitrogênio pelo método Brunauer-Emmett-Teller (BET), e microscopia de força atômica (MFA). A ferrita produzida foi usada como catalisador e sua atividade foi investigada na reação de foto-Fenton para a degradação de um corante orgânico têxtil (Vermelho Procion H-E7B) sob irradiação de luz visível. Nos experimentos, foram analisadas diferentes variáveis de processo, tais como concentrações de corante e peróxido de hidrogênio, pH e tempo. As constantes de velocidade das reações de foto-Fenton foram determinadas para ambos os materiais preparados pelas diferentes rotas. Os resultados das sínteses demonstraram a obtenção de partículas com diferentes propriedades físicas, tais como área superficial, volume e tamanho de poros. Os testes da reação foto-Fenton indicaram que o material preparado neste trabalho apresenta satisfatória atividade para a degradação do poluente orgânico, até 97% de remoção de cor e 60% de mineralização, em solução aquosa. Todas as variáveis do processo reacional estudadas influenciaram significativamente no processo catalítico.

Palavras-chave: Ferrita de zinco, Síntese, Solvotérmico, Microondas, Foto-Fenton.

ABSTRACT

In this work, zinc ferrite oxide was performed ($ZnFe_2O_4$) was synthesized by the solvothermal conventional method and the microwave-assisted solvothermal route. The influence of different synthesis as well as their variables on the physical properties of the material were investigated. The powders were characterized by X-ray diffraction (XRD), infrared spectroscopy (FTIR), nitrogen adsorption/desorption measurements by the Brunauer-Emmett-Teller method (BET), and atomic force microscopy (AFM). The produced ferrite was used as catalyst and its activity was investigated in the photo-Fenton reaction for the degradation of textile organic dye (Procion Red H-E7b) under visible light irradiation. In the experiments, different process variables such as dye and hydrogen peroxide concentrations, pH and reaction time were analyzed. The rate constants for the photo-Fenton reactions were determined for both materials prepared by different routes. The synthesis results demonstrated the formation of particles with different physical properties such as surface area, pore volume and size. The experiments of photo-Fenton reaction indicated that the materials prepared in this work present satisfactory activity for the degradation of organic pollutant, 97% de decolorization and 60% de mineralization, in aqueous solution. All studied variables of the reaction process significantly influenced on the catalytic process.

Keywords: Zinc Ferrite, Synthesis, Solvothermal, Microwave, photo-Fenton.

LISTA DE FIGURAS

LISTA DE TABELAS

LISTA DE ABREVISTURAS E SIGLAS

POAs Processos Oxidativos Avançados (AOPs)
DRX Difração de raios-X (XRD)
MFA Microscopia de força atômica (AFM)
BET Brunauer-Emmett-Teller
BJH Barret-Joyner-Halenda
DQO Demanda Química de Oxigênio
UV Ultravioleta
BV Bandas de valência
BC Bandas de condução
COT Carbono Orgânico Total (TOC)
FTIR Espectroscopia no Infravermelho por Transformada de Fourier
IUPAC União Internacional de Química Pura Aplicada
JCPDS Joint Committee on Powder Diffraction Standards

SUMÁRIO

CAPÍTULO 1

1.1 Introdução

Existe uma crescente preocupação mundial com o controle e redução de taxas de emissões de poluentes no meio ambiente, onde novas tecnologias e processos têm sido adotados a fim de um desenvolvimento sustentável e adequação às mudanças da legislação.

Recentemente, processos oxidativos avançados (POAs) têm sido amplamente aplicados na degradação de poluentes orgânicos em soluções aquosas. Dentre os POAs, a reação heterogênea de Fenton é um dos processos de maior interesse, que utilizam catalisadores à base de ferro, sendo a sua principal vantagem, a fácil recuperação do catalisador após o processo de tratamento. Estruturas de ferrita tem despertado muito interesse devido a sua gama de aplicações. É um material que tem sido utilizado em ferrofluidos, na biomedicina, como adsorvente e fotocatalisador para remoção de substâncias tóxicas, incluindo gases, tratamento de resíduos contendo metais pesados, corantes, etc.

Recentemente, partículas de ferrita de zinco ($ZnFe_2O_4$) tem despertado muita atenção devido ao seu potencial fotocatalítico e por terem propriedades magnéticas, podem ser separadas e recuperadas ao final do tratamento por um campo magnético. Dentre as vantagens de se utilizar a tecnologia de Fenton heterogêneo, é que esta não gera lodo, e assim, geralmente não se necessitam de processos de tratamento posteriores ou disposição. Pode se ressaltar também que esse tipo de processo pode ser uma complementação dos tratamentos convencionais já utilizados os quais não são completamente eficientes na descontaminação dos efluentes

Dessa forma, este trabalho visou desenvolver um material com atividade catalítica para a descontaminação de efluente sintético contaminado por corante têxtil. Diferentes rotas de sínteses foram empregadas para determinar os seus efeitos sobre as propriedades físicas do catalisador. Faz-se necessário o estudo das rotas de síntese para verificar o quanto a metodologia de preparo do material influencia na estrutura de poros, e onde essas características influenciam consideravelmente sobre a atividade do catalisador.

1.2 Objetivos

1.2.1 Objetivo Geral

Este estudo tem como objetivo geral avaliar as propriedades das partículas de ferrita de zinco obtidas por diferentes rotas de síntese, como a solvotérmica convencional e a solvotérmica assistida por microondas. Além disso, avaliar a atividade catalítica do material produzido através da reação heterogênea de foto-Fenton.

1.2.2 Objetivos Específicos

Para atender ao objetivo geral, faz-se necessário o cumprimento dos seguintes objetivos específicos:

1. Sintetizar partículas de $ZnFe_2O_4$ pelo método solvotérmico convencional;
2. Sintetizar partículas de $ZnFe_2O_4$ pelo método solvotérmico assistido por microondas;
3. Caracterizar as partículas sintetizadas através de difração de raios-X (DRX), infravermelho (FTIR); pelo método BET e microscopia de força atômica (MFA);

   Avaliar a atividade catalítica do material sintetizado pelas diferentes rotas na reação de foto-Fenton, avaliando algumas das diferentes variáveis envolvidas no processo reacional, descrevendo os efeitos.

1.3 Estrutura da Dissertação

Esta dissertação apresenta-se dividida em quatro capítulos. O primeiro capítulo descreve a relevância do assunto tratado na dissertação, os objetivos gerais e específicos e ainda a estrutura em que se apresenta. No segundo capitulo esta apresentada a revisão bibliográfica onde estão descritos os tratamentos empregados a efluentes têxteis, os processos oxidativos avançados e a ferrita de zinco bem como a síntese da mesma. O terceiro capítulo apresenta os resultados abordados nesse trabalho em formato de artigo sendo que esta um

artigo publicado e dois artigos submetidos. E por fim o ultimo capítulo trata das conclusões obtidas no decorrer dos experimentos.

CAPÍTULO 2

REVISÃO BIBLIOGRAFICA

Neste capitulo será apresentada uma revisão bibliográfica abrangendo o material ferrita de zinco, a síntese do mesmo, algumas técnicas de remoção de corantes, bem como a legislação aplicada a efluentes líquidos. Serão apresentados ainda os processos oxidativos avançados, em especial, a reação do tipo Fenton.

2.1 Tratamentos empregados a efluentes têxteis

A indústria têxtil tem um alto potencial poluidor devido à alta quantidade de matéria orgânica e coloração dos efluentes. A quantidade mundial de efluentes gerados atualmente em indústrias têxteis, de couro e de papel e celulose é, cerca de, 800 toneladas⁄dia de corantes, na forma de matéria dissolvida ou suspensa. Os processos de tratamento de efluentes ainda não são eficazes para a descontaminação total, sendo que apenas metade dos contaminantes é removida. A maioria dos corantes reativos é resistente às metodologias convencionais, como o biológico ou químico, devido ao grande número de anéis aromáticos presentes em suas moléculas (ARAUJO, 2008).

A indústria têxtil tem impactado o meio ambiente, em termos de descarga de poluentes e consumo de água e energia, que vem sendo reorganizado ao longo do tempo. A maioria dos contaminantes encontrados nos efluentes têxteis são sólidos suspensos, altos teores de demanda química de oxigênio, corantes com tonalidades intensas e outras substâncias solúveis. Os componentes desses processos diferem consideravelmente em sua composição, pois passam por processos, maquinários e indústrias diferentes (OLLER *et al.*, 2011).

No Brasil as indústrias buscam a adequação a legislação em vigor atualmente. A resolução número 430 do Conselho Nacional de Meio Ambiente – CONAMA, que dispõe sobre as condições e padrões de lançamento de efluentes, completa e altera a resolução número 357, os efluentes de qualquer fonte poluidora deverão ser lançados diretamente em

corpos receptores. As indústrias devem seguir as seguintes exigências onde os teores dos contaminantes nos efluentes devem estar nos seguintes teores:

- pH entre 5 e 9;
- temperatura inferior a 40˚C;
- materiais sedimentáveis até 1 mL⁄L em testes de 1 hora em tanques de sedimentação Inmhoff;
- a vazão máxima de lançamentos deve ser de 1,5 a vazão média do período de atividade diária do agente poluidor;
- óleos minerais até 20 mg⁄L, óleos vegetais e gorduras animais até 50 mg⁄L;
- ausência de materiais flutuantes; redução de 60% de Demanda Bioquímica de Oxigênio;
- a quantidade de ferro dissolvida permitida é de 15 mg⁄L e de nitrogênio é de 20 mg⁄L de solução.

As principais tecnologias empregadas no tratamento de efluentes têxteis são os tratamentos biológicos, coagulação, floculação, tecnologias envolvendo membranas, adsorção e processos oxidativos. Os processos biológicos envolvidos podem ser aeróbios, que removem corantes solúveis, e geralmente mineralizam o corante, ou anaeróbios, que promovem a descoloração por mecanismos de redução e a geração de metano. Ambos os processos são capazes de remover altos teores de DQO, porém não conseguem remover os corantes reativos, assim como os processos de coagulação e floculação (ARAUJO, 2008).

Os processos envolvendo membranas são muito eficientes na remoção de cor, podem ser reutilizadas, são eficientes para todos os tipos de corantes, porém necessitam de um alto custo de investimento. As membranas podem ser do tipo de osmose inversa, nanofiltração, ultrafiltração, de diálise ou de ionização. Outro processo que é bastante utilizado é o de adsorção, e nesse podem ser utilizados carvão ativado, sílica, carvão simples ou ainda, polímeros sintéticos. Porém, é considerado um processo lento e com alto custo de investimento e operação. Além desses, uma tecnologia emergente para a remoção deste tipo de poluente em efluentes industriais são os processos oxidativos avançados (POAs), que tem sido largamente usado nos últimos anos, o qual será descrito posteriormente (ARAUJO, 2008).

2.2 Processos Oxidativos Avançados

Processos oxidativos avançados é uma tecnologia emergente para a remoção de moléculas orgânicas de águas residuais, possuem alta estabilidade química e baixa degradabilidade, são geralmente utilizados em processos de pré-tratamento. Estes tipos de processos ocorrem em condições ambientes, tanto de temperatura quanto de pressão e possuem uma capacidade de geração de radicais altamente oxidantes, fazendo com que ocorra a oxidação completa de compostos orgânicos em moléculas como CO_2, H_2O e alguns sais inorgânicos (BOKARE e CHOI, 2014).

As principais vantagens que se podem mencionar quando se trata de processos oxidativos avançados é que eles não só trocam a fase do contaminante como o transformam quimicamente. Geralmente obtém-se a mineralização completa do contaminante, o que não ocorre com as tecnologias convencionais, não empregam tecnologias fortemente oxidantes e conseguem oxidar completamente as moléculas orgânicas.

Os POA's podem ser caracterizados de acordo com a fonte de geração dos radicais (·OH), sendo que os oxidantes utilizados podem ser o H_2O_2 e O_3. O H_2O_2, na maioria dos casos, deve ser utilizado junto com sais a base do metal de transição Fe^{2+}, O_3 e irradiação de UV (KARCI, 2014). Os processos oxidativos geralmente empregados são Fenton, Fenton foto assistido, fotocatálise, sistemas com ozônio. O mecanismo aceito quando se trata de um composto orgânico genérico (R) oxidado pelo radical hidroxila (·OH) pode ser representado por:

$$^{\cdot}OH + RH \rightarrow H_2O + R^{\cdot} \quad (1)$$

$$R^{\cdot} + H_2O_2 \rightarrow ROH + {}^{\cdot}OH \quad (2)$$

$$R^{\cdot} + O_2 \rightarrow ROO^{\cdot} \quad (3)$$

$$ROO^{\cdot} + RH \rightarrow ROOH + R^{\cdot} \quad (4)$$

A Tabela 01 demonstra de forma resumida as tecnologias dos processos oxidativos com ou sem radiação UV, em sistemas homogêneos que representam uma fase única e heterogêneos é onde há presença de fase sólida.

Tabela 01 - Tipos de processos oxidativos avançados

Sistemas	Homogêneos	Heterogêneos
Com radiação	$O_3/H_2O_2/UV$	$catalisador/UV$
	O_3/UV	$catalisador/H_2O_2/UV$
	H_2O_2/UV	
	$Fe^{2+}/H_2O_2/UV$	
Sem radiação	O_3/H_2O_2	$catalisador/H_2O_2$
	Fe^{2+}/H_2O_2	

Os processos oxidativos envolvem um a série de reações. Como o radical hidroxil envolvido é extremamente instável e reagem devido seu alto potencial de oxidação as reações são rápidas e não especificas. Quando envolvem moléculas orgânicas, e são controladas pela transferência de massa desse radical para as moléculas orgânicas ou ainda pela produção dos mesmos, geralmente apresentam uma cinética de primeira ordem. Alguns mecanismos são apresentados na Tabela 02 (MAHAMUNI e ADEWUYI, 2010).

Tabela 02 - Processos oxidativos e os mecanismos das reações. Adaptado de Mahamuni e Adewuyi, 2010.

Processo	Reações
O_3	$O_3 + OH^- \rightarrow OH_2^- + O_2$ $O_3 + OH_2^- \rightarrow OH_2^{\cdot} + O_3^-$
O_3/H_2O_2	$H_2O_2 + 2O_3 \rightarrow 2\ {}^{\cdot}OH + 3O_2$
O_3/UV	$O_3 + H_2O \overset{hv}{\rightarrow} 2\ {}^{\cdot}OH + O_2$
H_2O_2/UV	$H_2O \overset{hv}{\rightarrow} 2\ {}^{\cdot}OH$
$O_3/H_2O_2/UV$	$O_3 + H_2O_2 + H_2O \overset{hv}{\rightarrow} 4\ {}^{\cdot}OH + O_2$
$Fenton$	$H_2O_2 + Fe^{2+} \rightarrow Fe^{3+} + {}^{\cdot}OH + OH^-$
$Fotocatalise$	$TiO_2 \overset{hv}{\rightarrow} e^- + h^+$ $TiO_2(h^+) + H_2O \rightarrow TiO_2 + {}^{\cdot}OH + H^+$ $TiO_2(h^+) + HO \rightarrow TiO_2 + {}^{\cdot}OH$ $TiO_2(h^+) + RX \rightarrow TiO_2 + RX^{\cdot +}$

2.2.1 Fotocatálise heterogênea

Os fotocalisadores são utilizados em diversas áreas para eliminação de contaminantes da água e do ar, produção de H_2, controle de odores, inativação de bactérias, etc. São materiais importantes, pois convertem energia solar ou artificial (*hv*) para utilizar em processos de redução e oxidação. Quando os elétrons (e^-) sofrem irradiação são excitados da banda de valência (BV) para a banda de condução (BC) dos fotocatalisadores, deixando uma

lacuna (h^+), os (e^-) e os (h^+) possibilitam que ocorram os processos de oxidação e redução. A energia de *band-gap* do material determina o comprimento de onda que pode ser absorvido e a diferença entre a BV e a BC esta inversamente relacionada ao comprimento de onda da luz. Quando os processos fotocatalíticos ocorrem em meio aquoso, a água e os íons hidróxidos reagem com os (h^+) fotogerados para formar os radicais hidroxil (·OH), que é o oxidante primário na oxidação fotocatalítica de compostos orgânicos (CASBEER *et al.*, 2012). Um mecanismo das reações envolvidas em processos de fotocatálise esta representado na Figura 01, a seguir:

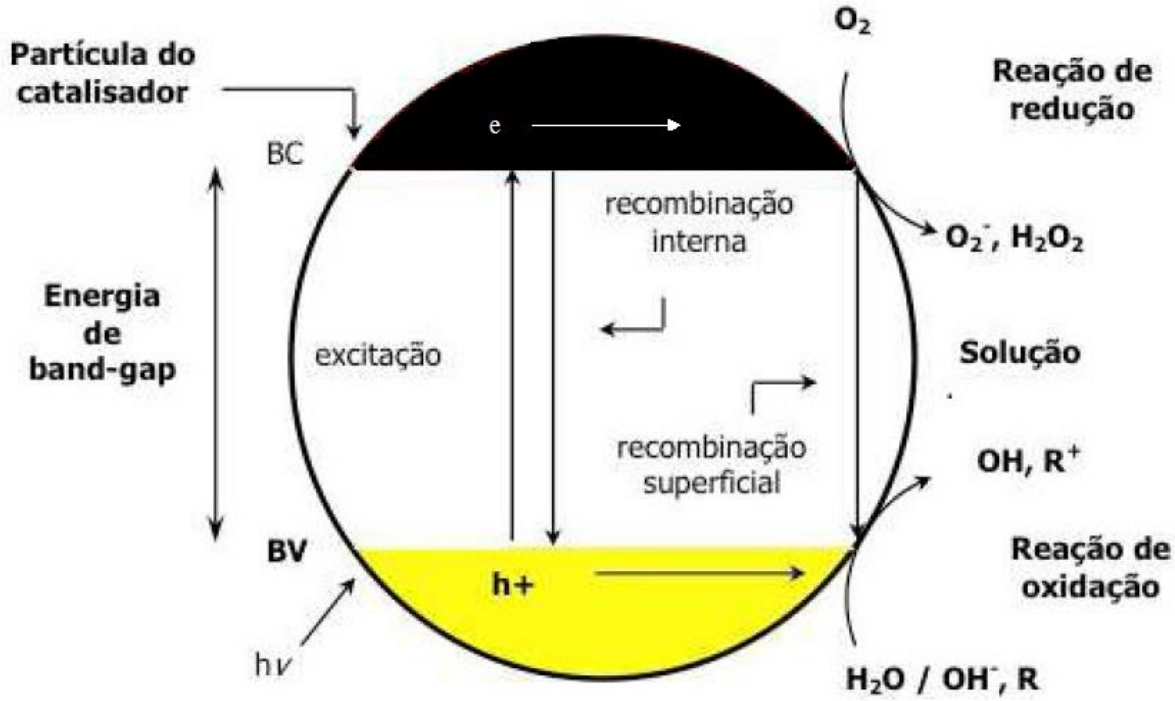

Figura 01 - Mecanismos das reações que ocorrem via fotocatálise para produzir ·OH para reagir com os contaminantes.

Vários fotocatalisadores vem sendo utilizados em processos de fotodegradação de compostos orgânicos, incluindo TiO_2, ZnO, Cu_2O, CdS, entre outros. A degradação fotoquímica de compostos orgânicos que vem sendo utilizada recentemente e vastamente estudada é H_2O_2/luz visível, sendo que a eficiência de degradação depende da taxa de decomposição do H_2O_2, com isso vem sendo pesquisado novos fotocalisadores (LU *et al.*, 2013).

Recentemente óxidos bimetálicos, compósitos de ferro e outro elemento metálico tem despertado muita atenção. Para reações catalíticas de decomposição de moléculas orgânicas é necessário um catalisador com alta atividade catalítica e alta estabilidade no meio reacional (ORBECI *et al.*, 2014). Espécies com oxigênio reativo possuem um papel crucial na fotocatálise heterogênea, a qual esta relacionada com a degradação de compostos orgânicos. Vários semicondutores e uma parte dos semicondutores em pó podem atuar como fotocatalisadores, os quais vêm sendo aplicados em uma série de problemas ambientais relacionados com a purificação de águas (VALENZUELA *et al.*, 2002).

2.2.2 Processos Fenton e foto-Fenton

Os processos que envolvem Fenton necessitam da formação de radicais ·OH a partir de H_2O_2, juntamente com sais de Fe^{2+} adicionados na solução, quando se trata de Fenton homogêneo. Devido ao alto potencial padrão de redução de 2,8 V dos radicais ·OH, apenas alguns dos compostos orgânicos, como os ácidos acéticos, maléico e oxálico, acetona e clorofórmio, por se tratarem de moléculas mais estáveis, não podem ser oxidados (PERA-TITUS *et al.*, 2004). Esse reagente foi descrito por Fenton em 1876, e embora ele não tenha descrito os mecanismos da reação envolvida, novas pesquisas mostraram que pode ser descrito conforme a seguinte equação:

$$Fe^{2+} + H_2O_2 \rightarrow Fe^{3+} + OH^- + \cdot\mathrm{OH} \quad (5)$$

Várias reações importantes ocorrem, e os íons férricos decompõem-se cataliticamente em presença de H_2O_2 em H_2O e O_2, formandos também radicais e íons ferrosos.

$$Fe^{3+} + H_2O_2 \rightleftharpoons FeOOH^{2+} + H^+ \quad (6)$$

$$FeOOH^{2+} \rightarrow Fe^{2+} + HO^{\cdot}{}_2 \quad (7)$$

$$Fe^{2+} + HO^{\cdot}{}_2 \rightarrow Fe^{3+} + HO_2^- \quad (8)$$

$$Fe^{3+} + HO^{\cdot}{}_2 \rightarrow Fe^{2+} + O_2 + H^+ \quad (9)$$

$$H_2O_2 + \cdot OH \rightarrow HO^{\cdot}{}_2 + H_2O \quad (10)$$

A eficiência nos processos de oxidação Fenton depende da razão de H_2O_2: carbono orgânico, a quantidade de matéria orgânica, temperatura e concentração de Fe (II). Dependendo do efluente a ser tratado, diferentes condições do processo podem ser empregadas para obter altos teores e eficiência de degradação. O pH, razão de Fe (II):H_2O_2 e concentração de H_2O_2 são cruciais para o processo (GUEDES *et al.*, 2003).

Os processos Fenton homogêneos possuem limitações importantes como a da faixa de pH, que pode variar de 2 a 3, e a produção de altas quantidades de lodo de ferro no fim do processo, o que faz com que aumentem os custos como o tratamento final das aguas residuais. Com isso, vem sendo desenvolvidas novas tecnologias pela aplicação do Fenton heterogêneo, onde vários materiais óxidos e hidróxidos de ferro vêm sendo utilizados para a degradação de contaminantes orgânicos, destacando-se os $CuFe_2O_4$, Fe_3O_4, α -Fe_2O_3 e α-FeOOH (WANG *et al.*, 2014; ZHANG *et al.*, 2014).

Quando se trata de processos de foto-Fenton, é necessário um catalisador com alta atividade e estabilidade no meio reacional. O pH afeta de forma moderada nessa reação, e em pH maiores do que 3, a eficiência degradativa diminui. Porém, o pH pode influenciar na lixiviação de partículas de ferro do catalisador heterogêneo, sendo que pH inferior a 3, a quantidade de lixiviado pode aumentar (ORBECI *et al.*, 2014).

A combinação dos reagentes Fenton e a luz UV-Vis gera radicais ·OH adicionais a partir da fotoredução de íons férricos em íons ferrosos e da fotólise do peróxido de hidrogênio (POURAN *et al.*, 2014). A taxa de decomposição de compostos orgânicos é acelerada na presença de radiação UV-Vis, a fotólise do Fe^{3+} (catalisador) em meio aquoso acelera a regeneração do Fe^{2+} (Equação 11) (VELOUTSOU *et al.*, 2014).

$$Fe^{3+} + H_2O \xrightarrow{hv} Fe^{2+} + H^+ + \cdot OH \quad (11)$$

Dentre as vantagens de se utilizar a tecnologia de Fenton heterogêneo, é que esta não gera lodo, e assim, geralmente não são necessários de processos de tratamento posteriores, e ainda são capazes de melhorar as propriedades organolépticas da agua tratada (DOMENECH *et al.*, 2001). Além disso, as partículas a base de ferro, por terem propriedades magnéticas, podem ser separadas e recuperadas ao final do tratamento por um campo magnético.

A seguir, na Tabela 03, estão apresentadas algumas das condições operacionais e catalisadores heterogêneos utilizados em reações do tipo Fenton e foto-Fenton.

Tabela 03 – Condições operacionais de degradação de compostos orgânicos a partir da Reação Fenton e foto-Fenton com catalisadores óxidos de ferro, adaptado de Pouran *et al.* 2014.

Composto	Catalisador	Condição Operacional					Condição Experimental/Comentários	Referencia
		[H2O2]	[Cat]	pH	T ˚C	λ nm		
Fenol (0,1 mM)	Magnetita /meso celular espuma de carbono (Fe_3O_4/MSU-F-C)	0,1 mM	0,1 gL^{-1}	3	25		95% de degradação de fenol em 4 h.	Chun *et al.*,2012
Bisfenol A 0,01 mM	Magnetita/ácido oxálico	0,5 mM	0.15gL^{-1}	3	23 - 25		Remoção complete do BPA, <120 com tempo de meia vida de 15 min.	Rodríguez *et al.*, 2009
Fenol (0,2 g L^{-1})	Maghemite/MCM-14 (MSFM)	0,98 mM	5 g L^{-1}	4	40		78% de remoção de COT em 2 h, decréscimo na remoção de COT para 65% apos três reciclos de reação.	Xia *et al.*, 2011
Vermelho Metil 50 mM	Quartz/oxido de ferro amorfo (III) (Q1), quartz/maghemite (Q2), quartz/magnetita (Q3), quartz/goetita (Q4)	0,98 mM		5; 7	20		Máxima oxidação do MR em pH 5 depois 7, >99% sorção do MR na superfície do catalisador, em 2 h maior taxa de degradação (min $^{-1}$) para Q4 nas duas faixas de pH.	Hanna *et al.*, 2008
Azul de metileno 100 mg L^{-1} (10 mL)	Niobia/compósito de oxido de ferro	2 mL/ 10 mL	30 mg		25		90% de descoloração utilizando niobia:oxido de ferro 1:1, 50% de descoloração utilizando niobia:oxido de ferro 1:5 em 120 min.	Oliveira *et al.*, 2007
Quinolone 10 mg L^{-1} (9,9 mL),	$Cu^{2+/}$goetita		10 mg				Degradação de Q em 240 min via hidroxilação sucessiva. Taxa de degradação alta comparada com goetita pura.	Guimaraes *et al.*, 2009

Bisfenol A – BPA, Vermelho Metil – MR, Azul de metileno – MB, Quinolone – Q.

Tabela 03 – Condições operacionais de degradação de compostos orgânicos a partir da Reação Fenton e foto-Fenton com catalisadores óxidos de ferro, adaptado de Pouran *et al.*, 2014 (Continua).

Composto	Catalisador	Condição Operacional					Condição Experimental/Comentários	Referencia
		$[H_2O_2]$	[Cat]	pH	T °C	λ nm		
2-chlorofenol $[H_2O_2]$	Goetita		0,5 g L^{-1}	3	50		Remoção de 2-CP e de COT de 99% e 75% respectivamente em 6 h.	
Pentaclorofenol, 0,0375 Mm	Goetita e hematita		0,4 g L^{-1}			<370	68% de degradação de PCP em suspensão de hematita e 83% em goetita em 1 h, menor degradação de PCP sob luz UV e sem acido oxálico.	Lan *et al.*, 2010
Farmacêuticos 420 mL, 10 mg L^{-1} [COT] 42 mg L^{-1}	Goetita Imobilizada	2mL/10 mL 5,8 – 2,9	0,05 g L^{-1}	3	25± 2		100% de degradação dos fármacos selecionados em 6 h, remoção de 12.5% e 21% de COT utilizando H_2O_2/COT razão mássica de 2,9 e 5,8 respectivamente.	Molina *et al.*, 2012
2,4,6-trinitrotolueno 0,11 mM	Hematita, ferridrita, lepidocracita, goetita, Magnetita, pirita, ferrugem verde.	3% (w/v)	2 g L^{-1}	7			Remoção de 60% de TNT com ferrugem verde (38,9% Fe II) seguido de pirita (46.6% Fe II) e magnetita (24.2% Fe II), baixa remoção de TNT com ferridrita, lepidocracita e hematita (Fe III).	Matta *et al.*, 2008
	Magnetita [EDTA] 10 mM [CMCD] 5 mM,	3% (w/v)	5% (w/w)	7			25% de remoção de TNT com magnetita sem agente quelante aumentou a degradação para 50% e 62% com EDTA e 50% e 62% com EDTA e CMCD respectivamente.	
Sulfadiazina 20 mg L^{-1} (250 mL)	Goetita	0,5 mM	0,4 gL^{-1}	3.5	30	350	3%, 15% e 93% de remoção de SD via UV, UV/goetita, UV/goetita/ oxalato respectivamente após 40 min de irradiação.	Wang *et al.*, 2010

2-chlorofenol – 2-CP, Pentaclorofenol – PCP, 2,4,6-trinitrotolueno – TNT, Sulfadiazina - SD

Tabela 03 – Condições operacionais de degradação de compostos orgânicos a partir da Reação Fenton e foto-Fenton com catalisadores óxidos de ferro, adaptado de Pouran *et al.*, 2014 (Continua).

Composto	Catalisador	Condição Operacional					Condição Experimental/Comentários	Referencia
		[H2O2]	[Cat]	pH	T ˚C	λ nm		
Etileno clorado & Benzeno, tolueno, etilbenzeno em fase não aquosa, fase aquosa 1,0 mM (250 mL)	Goetita (α-FeOOH) [HC] 1,0 mM (250 mL)	0,01 e 0,5%	0,22 g 4 gL^{-1} Fe	3,5	25 ± 3		% de remoção do etilbenzeno > tolueno > Benzeno, baixo percentual de remoção para compostos com alta solubilidade em agua.	Yeh *et al.*,2008
Ácido benzoico 50 mg L^{-1}	Hematita-SBA-15	162 mg L^{-1}	0,6 gL^{-1}	3,1	27 ± 3	365	100% de remoção de BA e 87.9% de COD depois de 240 min, 93% H_2O_2 consumido, Eficiência COD/H_2O_2 consumida de 0,66.	Pariente *et al.*, 2008
Azul de metileno 50 mg L^{-1}	Cr-magnetite $Fe_{3-x}Cr_xO_4$ (15 mg)	0,3 mg L^{-1}		6	25 ± 1		Maior taxa de degradação em menor quantidade de Cr, decaimento na taxa de descoloração e remoção de COT com o aumento da quantidade de Cr devido ao decréscimo de Fe^{2+}.	Magalhães *et al.*, 2007
Tetrabromobisfenol A 20 mg L^{-1}	Titanomagnetita $Fe_{2,02}Ti_{0,98}O_4$ 0,125 g L^{-1}	10 mmol L^{-1}		6,5	25		Degradação >97% TBBPA no UV/ Sistema $Fe_{2.02}Ti_{0.98}O_4/H_2O_2$, 75% no sistema UV/$H_2O_2$tr	Zhong *et al.*, 2012
Azul de Metileno 100 mg L^{-1}	$Fe_{2,46}Ni_{0,54}O_4$ $Fe_{2,47}Mn_{0,53}O_4$ $Fe_{2,25}Co_{0,75}O_4$ (30 mg)	2,5 mol L^{-1}			25 ± 1	633	10% de remoção de cor em 50 min utilizando $Fe_{2,46}Ni_{0,54}O_4$, descoloração completarem 5 e 10 min	Costa *et al.*, 2003

Etileno clorado - PCE,TCE, cis 1,2-DCE, trans1,2-DCE, 1,1 DCE, fase aquosa – HC, Acido benzoico – BA, Azul de metileno – MB, Tetrabromobisfenol A - TBBPA

Tabela 03 – Condições operacionais de degradação de compostos orgânicos a partir da Reação Fenton e foto-Fenton com catalisadores óxidos de ferro, adaptado de Pouran *et al.*, 2014 (Continua)

Composto	Catalisador	Condição Operacional [H_2O_2]	[Cat]	pH	T ˚C	λ nm	Condição Ótima	Referencia
Clorobenzeno 30 mg L^{-1}	Mn-magnetite $Fe_{3-x}Mn_xO_4$ (30 mg)	2,5 mol L^{-1}			25 ± 1		14, 7, 5 e <1% degradação de clorobenzeno para reações utilizando $Fe_{2,47}Mn_{0,53}O_4$.	Costa *et al.*, 2003; Oliveira *et al.*, 2000
Azul de metileno UV 0,2 mmol L^{-1} (500 mL)	TieV-magnetite $Fe_{3-x-x0}Ti_xV_x{\cdot}O_4$ (1.0 g L^{-1})	10 mmol L^{-1}		7	25	365	Aumento na descoloração do MB de 48% ate 96% com aumento de Ti de x ¼ 0,0 ate x ¼ 0,69 após 120 min.	Liang *et al.*, 2012
Azul de metileno 100 mg L^{-1}(400 mL)	Titanomagnetite $Fe_{3-x}Ti_xO_4$ (1,0 g L^{-1})	0,30 mol L^{-1}		6,8	30		Alta atividade do Ti-magnetita depois magnetite pura. Diminuição do MB residual com o aumento de Ti.	Yang *et al.*, 2009
Azul de metileno 0,2 mmol L^{-1} (200 mL)	V-magnetite $Fe_{3-x}V_xO_4$ $0 \leq x \leq 0{,}34$g L^{-1})	100 mmol L^{-1}		10	25		Remoção de 41, 60, 81 e 93% da cor do MB em 11 h utilizando Fe_3O_4, $Fe_{2,84}V_{0,16}O_4$, $Fe_{2,74}V_{0,26}O_4$ e $Fe_{2,66}V_{0,34}O_4$, respectivamente.	Liang *et al.*, 2010
4-clorofenol	$Ni_xZn_{1-x}Fe_2O_4$ x = 0,0, 0,25, 0,5, 0,75, 1.0	39,16 mM	20g L^{-1}	6,67-6,86	70		Eficiente na degradação oxidativa do 4-clorofenol, remoção de 99,1% de DQO	Kurian, M. e Nair, D. S., 2014
Azul de Metileno 0,1 g L^{-1}	g-Fe_2O_3 a-Fe_2O_3 $Fe_{3\_x}M_xO_4$ (M ¼ Co & Mn) (30 mg)	0.3 mol L^{-1} (10 mL)		5-6,5	25		Nenhuma descoloração significativa com oxido Fe_2O_3, completa remoção de cor com alta oxidação através de $Fe_{3\_x}M_xO_4$ em 5e10 min.	Costa *et al.*, 2006
Clorobenzeno 0,02 g L^{-1}	Mn-magnetite $Fe_{3-x}Mn_{xO4}$ (30 mg)	0,3 mol L^{-1} ou 10,2 g L^{-1}			25 ± 1		1, 5, 7 e 14% de remoção de CBZ utilizando Fe_3O_4, $Fe_{2.79}Mn_{0,21}O_4$, $Fe_{2,74}Mn_{0,26}O_4$ e $Fe_{2,47}Mn_{0,53}O_4$ respectivamente em 30 min.	

Clorobenzeno – CBZ, Azul de metileno – MB

2.3 Ferrita de zinco

Espinélios de ferrita possuem geralmente uma fórmula do tipo MFe_2O_4, onde M representa o cátion de um metal, e são quimicamente, fisicamente e magneticamente estáveis. As propriedades das ferritas estão fortemente ligadas à quantidade e natureza dos sítios metálicos incorporados a sua estrutura. Alguns cátions podem aumentar ou diminuir a estabilidade do catalisador, e assim, o Zn^{+2} tem a capacidade de aumentar a estabilidade. Com o aumento da estabilidade, as partículas de ferrita são capazes de realizar a fotoredução e fotooxidação, o que é necessário para que ocorra a completa decomposição de composto orgânico, e ao mesmo tempo absorver a luz visível de forma eficaz (CASBEER *et al.*, 2012).

Quando se incorpora o cátion Zn^{2+} como metal de transição em estruturas de Fe^{2+} $Fe_2{}^{3+}O_4$, considera-se que podem formar estruturas promissoras para reduzir compostos gasosos como CO, CH_4, etc, (KOSEOGLU *et al.*, 2008). Com isso, partículas de $ZnFe_2O_4$ despertam interesse, pois tem potencial para serem aplicadas.

As ferritas oferecem uma vantagem de terem uma energia de *band gap* que absorvem no comprimento da luz visível, e assim, como todos os espinélios, possuem estrutura cristalina, contribuindo para um aumento em sua eficiência devido à disponibilidade de sítios catalíticos extras. Recentemente, surgiu o interesse de utilizar ferritas como fotocatalisadores de luz visível para a degradação de águas contaminadas, devido ao fato de existirem poucos materiais com capacidade de oxidar e reduzir, que é necessário para a decomposição completa de compostos orgânicos (CASBEER *et al.*, 2012).

Uma situação emergente em processos oxidativos avançados é o estudo da aplicação de catalisadores magnéticos para a degradação de poluentes, sendo que as propriedades magnéticas abriram acesso para aplicação de estudos em engenharia de processos de separações. As partículas podem ser separadas com base em suas nanoestruturas e, dependendo do ordenamento dos átomos na estrutura magnética, irão facilitar a direção da magnetização (MAHMOODI, 2013). Pesquisas baseadas em partículas de $ZnFe_2O_4$ apresentaram características de grande relevância, como propriedades magnéticas e eletromagnéticas, as quais podem influenciar em aplicações de descontaminação de águas residuais, já que o material pode ser removido do efluente por um campo magnético, facilitando o processo de separação e posterior reutilização do catalisador. Ainda, se destacam por descartar limitações em reações do tipo Fenton, como a não formação de lodo e operações em pH neutro (CASBEER *et al.*, 2012; ANCHIETA *et.al*, 2014).

2.3.1 Síntese do Material

Sabe-se que a rota de síntese pode influenciar nas propriedades do material produzido, e em alguns métodos pode ocorrer a formação de fases indesejáveis. Algumas das rotas de síntese da ferrita de zinco, bem como algumas das aplicações estudadas atualmente, estão dispostas na Tabela 04, a seguir. As rotas de precipitação e hidrotérmica são as mais usuais. As mais diversas rotas de síntese de ferrita de zinco são reportadas, e dentre elas, estão a cooprecipitação, hidrotérmica, sol-gel, combustão e a solvotérmica, sendo que algumas podem ser assistidas por micro-ondas ou ultrassom.

A perspectiva de intensificação de processos está sendo considerada promissora e de grande relevância para a indústria de processos químicos e engenharia química moderna, pois visa à redução de impactos ambientais e de consumo de energia e, ainda, conservação de recursos naturais, significando o aprimoramento de técnicas e equipamentos de processamentos químicos. A energia de microondas está sendo proposta como intensificação de processo, sendo capaz de maximizar a eficácia intra e intermolecular, onde cada molécula é capaz de sofrer a mesma transformação, otimiza as forças motrizes em qualquer escala, e maximiza a área superficial e efeitos sinérgicos dos processos (ROSA *et al.*, 2013).

As rotas de síntese térmicas envolvem os métodos hidrotérmico, solvotérmico, micro-ondas e hidrotérmico com semente, onde todos esses utilizam Fe $(NO_3)_3.9H_2O$ ou $FeCl_3.6H_2O$ e um outro sal de metal, utilizado geralmente M-$(NO_3)_2$, M-SO_4 ou M-Cl_2, onde M é o metal usado na síntese. Os sais são dissolvidos em água ou em outro solvente e o pH é ajustado entre 7 e 12. A mistura é colocada em autoclaves e aquecida por um intervalo de tempo de 12-24 h e, posteriormente, deixada resfriar em temperatura ambiente. Os sólidos são coletados, filtrados e secos a 85˚C. No método hidrotérmico com sementes, é utilizado uma semente do metal utilizado (M_2O_3) juntamente com o sal de Fe (III), e os compostos são colocados nas autoclaves e aquecido seguidos do mesmo procedimento mencionado anteriormente. Partículas de ferrita de zinco podem ser sintetizadas a partir da rota solvotérmica, formando uma única fase, sendo que as condições empregadas no processo podem variar. Por exemplo, a faixa de temperatura pode ser de 120˚C a 150˚C sobre uma larga faixa de tempo de reação variando de 1 a 48 h, sendo que as características do material podem ser influenciadas por esses parâmetros (SURINWONGA e RUJIWATRA, 2013).

O método sol-gel consiste na adição dos precursores em ácido cítrico para que ocorra a formação do gel. Os precursores são dissolvidos em água e etanol, e agitados vigorosamente

em pH próximo de 9, para a formação do gel. Logo após, o gel é seco e sintetizado na faixa de 450 a 800˚C em vários períodos de tempo. Já, o método de co-precipitação é similar aos métodos térmicos. Fe (III) e os sais metálicos são dissolvidos em água através de surfactantes, ácido olêico sob agitação e aquecimento suave. O pH é aumentado de 7 a 10 para que ocorra a precipitação das partículas, e essas são filtradas, lavadas com água destilada e etanol, secas a 100˚C, por fim, calcinadas.

As reações em estado sólido envolve o aquecimento dos pós dos sais metálicos e de ferro, geralmente em temperaturas acima de 1000 ˚C por um período de 2 h (CASBEER *et al.*, 2012). Nesse trabalho, selecionou-se a rota solvotérmica convencional e solvotérmica assistida por micro-ondas para a síntese da ferrita de zinco.

Tabela 04 – Rotas de síntese utilizadas para ferrita de zinco e aplicações.

Síntese	Aplicação	Referencia
sol-gel	-	PATIL *et al.*, 2013
	atividade de redução, semicondutores	CASBEER *et al.*, 2012; LIU *et al.*, 2009
	desidrogenação 1-butano	TOLEDO-ANTONIO *et al.*, 2002
	semicondutores, sensores a gás	XIANGFENG. *et al.*, 1999
Precipitação e co-precipitação	remoção benzotriazolo por Fenton fotoelétrico	WU *et.al*, 2013
	fotodegradação ou degradação de poluentes orgânicos	XIEA *et al.*, 2013; MAHMOODI, 2013;CASBEER *et al.*, 2012
Hidrotérmico	Fenol fotodegradação de corante Rodamina B	VALENZUELA *et.al*, 2002 ZHANG *et al.*, 2010
	fotodegradação de Reactive Red 198 e Reactive Red 120	MAHMOODI, 2013
	degradação de compostos orgânicos	LI *et al.*,1996; SINGH *et al.*, 2013; MALETIN *et al.*, 2007
Hidrotérmico c/ micro-ondas	fotodegradação de poluentes orgânicos	CAO *et al.*, 2009
Solvotérmica	fotodegradação de poluentes orgânicos	LU *et al.*, 2013; ANCHIETA *et.al*, 2014; KOSEOGLU *et al.*, 2008
Solvotérmica c/ ultrassom	fotodegradação poluentes orgânicos -	LI *et al.*,2011 SURINWONGA *et al.*, 2012
Combustão em micro-ondas	-	KOOTI *et al.*, 2012
Reações em estado sólido	Degradação fotocatalítica de moléculas orgânicas e inorgânicas e ainda atividade antimicrobiologica	CASBEER *et al.*, 2012

REFERENCIAS

ANCHIETA, C. G.; SALLET, D.; FOLETTO, E. L.; SILVA, S. S.da; CHIAVONE-FILHO, O.; NASCIMENTO, C. A. O. do; **Synthesis of ternary zinc spinel oxides and their application in the photodegradation of organic pollutant.** Ceramics International, v. 40, p. 4173–4178, 2014.

ARAUJO, V. F. **Estudo do processo Fenton Heterogêneo utilizando hematita (FeO) como catalisador na descoloração de soluções de corante reativo.** Tese de Doutorado - Universidade Federal do Rio de Janeiro, Escola de Química. 2008

BOKARE, A. D.; CHOI, W. **Review of iron-free Fenton-like systems for activating H_2O_2 in advanced oxidation processes.** Journal of Hazardous Materials, v. 275, p. 121–135, 2014.

CAO S.; ZHUA Y.; CHENGA G.; HUANG Y. **$ZnFe_2O_4$ nanoparticles: Microwave-hydrothermal ionic liquid synthesis and photocatalytic property over phenol.** Journal of Hazardous Materials, v. 171, p. 431–435, 2009.

CASBEER E.; SHARMA V. K.; LI X. **Synthesis and photocatalytic activity of ferrites under visible light: A review.** Separation and Purification Technology, v. 87, p. 1–14, 2012.

COSTA, R.C.C.; LELIS, M.D.F.F.; OLIVEIRA, L.C.A.; FABRIS, J.D.; ARDISSON, J.D.; RIOS, R.R.V.A.; SILVA, C.N.; LAGO, R.M. **Remarkable effect of Co and Mn on the activity of $Fe_{3-x}M_xO_4$ promoted oxidation of organic contaminants in aqueous medium with H_2O_2.** Catalysis Commun, v. 4, p. 525 - 529, 2003.

COSTA, R.C.C.; LELIS, M.F.F.; OLIVEIRA, L.C.A.; FABRIS, J.D.; ARDISSON, J.D.; RIOS, R.R.V.A.; SILVA, C.N.; LAGO, R.M. **Novel active heterogeneous Fenton system based on $Fe_{3-x}M_xO_4$ (Fe, Co, Mn, Ni): the role of M2þ species on the reactivity towards H_2O_2 reactions. J. Hazard.** Material, v. 129, p. 171 - 178, 2006.

CHUN, J., LEE, H., LEE, S.-H., HONG, S.-W., LEE, J., LEE, C., LEE, J. **Magnetite/ mesocellular carbon foam as a magnetically recoverable Fenton catalyst for removal of phenol and arsenic.** Chemosphere, v. 89, p. 1230 – 1237, 2012.

DOMÈNECH, X.; JARDIM, W.F.; LITTER, M.I. **Processos avanzados de oxidación para la emininación de contaminantes.** In: BLESA, M. A. *Eliminación de contaminantes por fotocatálisis heterogênea*, La Plata: Digital Graf., 2001

GUEDES, A. M. F. M.; MADEIRA L. M.P.; BOAVENTURA, R.A.R.; COSTA, C. A.V. **Fenton oxidation of cork cooking wastewater—overall kinetic Analysis.** Water Research, v. 37, p. 3061–3069, 2003.

GUIMARAES, I.R.; GIROTO, A.; OLIVEIRA, L.C.A.; GUERREIRO, M.C.; LIMA, D.Q.; FABRIS, J.D. **Synthesis and thermal treatment of cu-doped goethite: oxidation of quinolone through heterogeneous Fenton process.** Applied Catalysis B: Environmental, v. 91, p. 581 - 586, 2009.

HANNA, K.; KONE, T.; MEDJAHDI, G. **Synthesis of the mixed oxides of iron and quartz and their catalytic activities for the Fenton-like oxidation.** Catalysis Commun, v. 9, p. 955 - 959, 2008.

KARCI, A. **Review - Degradation of chlorophenols and alkylphenol ethoxylates, two representative textile chemicals, in water by advanced oxidation processes: The state of the art on transformation products and toxicity.** Chemosphere, v. 99, p. 1–18, 2014.

KOOTI M.; SEDEH A. N.; **Glycine-assisted fabrication of zinc and manganese ferrite nanoparticles**. Scientia Iranica F , v. 19, n. 3, p. 930–933, 2012.

KOSEOGLU Y.; BAYKAL A.; TOPRAK M. S.; GOZUAK F.; BASARAN A. C.; AKTAS B.; **Synthesis and characterization of $ZnFe_2O_4$ magnetic nanoparticles via a PEG-assisted route**. Journal of Alloys and Compounds, v. 462, p. 209–213, 2008.

KURIAN, M.; NAIR, D. S. **Heterogeneous Fenton behavior of nano nickel zinc ferrite catalysts in the degradation of 4-chlorophenol from water under neutral conditions**. Journal of Water Process Engineering, inpress, 2014

LAN, Q.; LI, F. B.; SUN, C. X.; LIU, C. S.; LI, X. Z. **Heterogeneous photodegradation of pentachlorophenol and iron cycling with goethite, hematite and oxalate under UVA illumination.** Journal of Hazardous Materials, v. 174, p. 64 – 70, 2010.

LI X.; LU G.; LI S.; **Synthesis and characterization of fine particle $ZnFe_20_4$ powders by a low temperature method**. Journal of Alloys and Compounds, v. 235, p. 150-155, 1996.

LI Y.; HOU Y.; ZHAO Q.; WANG L.; **A general, one-step and template-free synthesis of sphere-like zinc ferrite nanostructures with enhanced photocatalytic activity for dye degradation**. Journal of Colloid and Interface Science, v. 358, p. 102–108, 2011.

LIANG, X.; ZHU, S.; ZHONG, Y.; ZHU, J.; YUAN, P.; HE, H.; ZHANG, J. **The remarkable effect of vanadium doping on the adsorption and catalytic activity of magnetite in the decolorization of methylene blue.** Applied Catalysis B: Environmental, v. 97, p. 151 - 159, 2010.

LIANG, X.; ZHONG, Y.; ZHU, S.; MA, L.; YUAN, P.; ZHU, J.; HE, H.; JIANG, Z. **The contribution of vanadium and titanium on improving methylene blue decolorization through heterogeneous UV-Fenton reaction catalyzed by their codoped magnetite.** Journal of Hazardous Materials, v. 199 - 200, p. 247 - 254, 2012.

LIU F.; LI X.; ZHAO Q.; HOU Y.; QUAN X.; CHEN G.; **Structural and photovoltaic properties of highly ordered $ZnFe_2O_4$ nanotube arrays fabricated by a facile sol–gel template meth od**. Acta Materialia, v. 57, p. 2684–2690, 2009.

LU, D.; Ma Y.; KUMAR, M.; LIN, J. **Photo-Fenton pretreatment of carbofuran – Analyses via experimental design,detoxification and biodegradability enhancement**. Separation and Purification Technology, v. 81, p. 325–331, 2011.

LU D.; ZHANG Y.; LIN S.; WANGL.; WANG C.; **Synthesis of magnetic ZnFe2O4/graphene composite and its application in photocatalytic degradation of dyes.** Journal of Alloys and Compounds, v. 579, p. 336–342, 2013.

MALETIN M.; MOSHOPOULOU E. G.; KONTOS A.G.; DEVLIN E.; DELIMITIS A.; ZASPALIS V.T.; NALBANDIAN L.; SRDIC V.V.; **Synthesis and structural characterization of In-doped $ZnFe_2O_4$ nanoparticles**. Journal of the European Ceramic Society, v. 27, p. 4391–4394, 2007.

MAGALHÃES, F.; PEREIRA, M.C.; BOTREL, S.E.C.; FABRIS, J.D.; MACEDO, W.A.; MENDONCA, R.; LAGO, R.M.; OLIVEIRA, L.C.A. **Cr-containing magnetites $Fe_{3x}Cr_xO_4$: the role of Cr^{3+} and Fe^{2+} on the stability and reactivity towards H_2O_2 reactions.** Applied Catalysis A: General, v. 332, p. 115 – 123, 2007.

MAHAMUNI, N. N.; ADEWUYI, Y. G. **Advanced oxidation processes (AOPs) involving ultrasound for waste water treatment: A review with emphasis on cost estimation.** Ultrasonics Sonochemistry, v. 17, p. 990–1003, 2010.

MAHMOODI N. M.; **Zinc ferrite nanoparticle as a magnetic catalyst: Synthesis and dye degradation**. Materials Research Bulletin, v. 48, p. 4255–4260, 2013.

MATTA, R.; HANNA, K.; KONE, T.; CHIRON, S. **Oxidation of 2,4,6-trinitrotoluene in the presence of different iron-bearing minerals at neutral pH.** Chemical Engineering Journal, v. 144, p. 453 - 458, 2008.

MOLINA, R.; SEGURA, Y.; MARTÍNEZ, F.; MELERO, J.A**. Immobilization of active and stable goethite coated-films by a dip-coating process and its application for photo-Fenton systems.** Chemical Engineering Journal, v. 203, p. 212 - 222, 2012.

OLIVEIRA, L.C.A.; LAGO, R.M.; RIOS, R.V.R.A.; AUGUSTI, R.; SOUSA, P.P.; MUSSEL, W.N.; FABRIS, J.D. **The effect of Mn substitution on the catalytic properties of ferrites.** In: Avelino Corma, F.V.M.S.M., José Luis, G.F. (Eds.), Studies in Surface Science and Catalysis. Elsevier, p. 2165 - 2170, 2000.

OLIVEIRA, L.C.A.; GONÇALVES, M.; GUERREIRO, M.C.; RAMALHO, T.C.; FABRIS, J.D.; PEREIRA, M.C.; SAPAG, K. **A new catalyst material based on niobia/iron oxide composite on the oxidation of organic contaminants in water via heterogeneous Fenton mechanisms.** Applied Catalysis A: General, v. 316, p. 117 - 124, 2007.

OLLER I.; MALATO S.; SÁNCHEZ-PÉREZ J.A. **Combination of Advanced Oxidation Processes and biological treatments for wastewater decontamination—A review.** Science of the Total Environment, v. 409, p. 4141–4166, 2011.

ORBECI, C.; UNTEA I.; NECHIFOR, G.; SEGNEANU A. E.; CRACIUN M. E. **Effect of a modified photo-Fenton procedure on the oxidative degradation of antibiotics in aqueous solutions**. Separation and Purification Technology, v. 122, p. 290–296, 2014;

ORTIZ DE LA PLATA, G.B.; ALFANO, O.M.; CASSANO, A.E. **Optical properties of goethite catalyst for heterogeneous photo-Fenton reactions: comparison with a titanium dioxide catalyst.** Chemical Engineering Journal, v. 137, p. 396 - 410, 2008.

PATIL R.P.; DELEKAR S.D.; MANE D.R.; HANKARE P.P.; **Synthesis, structural and magnetic properties of different metal ion substituted nanocrystalline zinc ferrite**. Results in Physics, v. 3, p. 129–133, 2013.

PARIENTE, M.I.; MARTÍNEZ, F.; MELERO, J.A.; BOTAS, J.A.; VELEGRAKI, T.; XEKOUKOULOTAKIS, N.P.; MANTZAVINOS, D. **Heterogeneous photo-Fenton oxidation of benzoic acid in water: effect of operating conditions, reaction by-products and coupling with biological treatment.** Applied Catalysis B: Environmental, v. 85, p. 24 - 32, 2008.

PERA-TITUS, M.; GARCÍA-MOLINA, V.; BAÑOS, M. A.; GIMÉNEZ, J.; ESPLUGAS, S. **Degradation of chlorophenols by means of advanced oxidation process: a general review.** Applied Catalysis B: Environmental, v. 47, p. 219-256, 2004.

POURAN, S. R.; RAMAN, A. A. A.; DUAD, W. M. A. W. **Review on the application of modified iron oxides as heterogeneous catalysts in Fenton reactions**. Journal of Cleaner Production, v.64, p. 24 – 35, 2014.

RODRÍGUEZ, E.; FERNÁNDEZ, G.; LEDESMA, B.; ÁLVAREZ, P.; BELTRÁN, F.J. **Photocatalytic degradation of organics in water in the presence of iron oxides: influence of carboxylic acids.** Applied Catalysis B: Environmental, v. 92, p. 240 - 249, 2009.

ROSA R.; VERONESI P.; LEONELLI C.; **A review on combustion synthesis intensification by means of microwave energy.** Chemical Engineering and Processing, v. 71, p. 2 – 18, 2013.

SINGH J. P.; DIXIT G.; SRIVASTAVA R. C.; NEGI P.; AGRAWAL H.M.; KUMAR R.; **HRTEM and FTIR investigation of nanosized zinc ferrite irradiated with 100 MeV oxygen ions**. Spectrochimica Acta Part A: Molecular and Biomolecular Spectroscopy, v. 107, p. 326–333, 2013.

SURINWONG, S.; RUJIWATRA, A. **Ultrasonic cavitation assisted solvothermal synthesis of superparamagnetic zinc ferrite nanoparticles.** Particulogy, v. 11, n. 5, p. 588–593, 2013.

TOLEDO-ANTONIO J.A.; NAVA N.; MART´INEZ M.; BOKHIMI X.; **Correlation between the magnetism of non-stoichiometric zinc ferrites and their catalytic activity for oxidative dehydrogenation of 1-butene.** Applied Catalysis A: General, v. 234, p. 137–144, 2002.

VALENZUELA M.A.; BOSCH P.; JIMÉNEZ-BECERRILL J.; QUIROZ O.; PÁEZ A.I. **Preparation, characterization and photocatalytic activity of ZnO, Fe2O3 and $ZnFe_2O_4$**. Journal of Photochemistry and Photobiology A: Chemistry, v. 148, p. 177–182, 2002.

VELOUTSOU, S.; Bizani, E.; Fytianos, K. **Photo-Fenton decomposition of b-blockers atenolol and metoprolol; study and optimization of system parameters and identification of intermediates.** Chemosphere, v. 107, p. 180–186, 2014.

WANG, Y.; ZHAO, H.; LI, M.; FAN, J.; ZHAO, G. **Magnetic ordered mesoporous copper ferrite as a heterogeneous Fenton catalyst for the degradation of imidacloprid.** Applied Catalysis B: Environmental, v. 147, p. 534– 545, 2014.

WANG, Y.; LIANG, J.B.; LIAO, X.D.; WANG, L. S.; LOH, T.C.; DAI, J.; HO, Y.W. **Photodegradation of sulfadiazine by goethite-oxalate suspension under UV light irradiation.** Industrial Engineering Chemistry Research, v. 49, p. 3527 - 3532, 2010.

WU J.; PU W.; YANG C.; ZHANG M.; ZHANG J. **Removal of benzotriazole by heterogeneous photoelectro-Fenton like process using $ZnFe_2O_4$ nanoparticles as catalyst.** Journal of Environmental Sciences, v. 25, n. 4, p. 801–807, 2013.

XIA, M., CHEN, C., LONG, M., CHEN, C., CAI, W., ZHOU, B. **Magnetically separable mesoporous silica nanocomposite and its application in Fenton catalysis**. Microporous Mesoporous Materials, v. 145, p. 217 – 223, 2011.

XIANGFENG C.; XINGQIN L.; GUANGYAO M. **Preparation and gas sensitivity properties of $ZnFe_2O_4$**. Sensors and Actuators B, v. 55, p. 19–22, 1999.

XIEA T.; XUA L.; LIUB C.; WANG Y.; **Magnetic composite $ZnFe_2O_4/SrFe_{12}O_{19}$: Preparation, characterization, and photocatalytic activity under visible light**. Applied Surface Science, v. 273, p. 684– 691, 2013.

YANG, S.; HE, H.; WU, D.; CHEN, D.; LIANG, X.; QIN, Z.; FAN, M.; ZHU, J.; YUAN, P. **Decolorization of methylene blue by heterogeneous Fenton reaction using $Fe_{3-x}Ti_xO_4$ ($0< x< 0.78$) at neutral pH values.** Applied Catalysis B: Environmental, v. 89, p. 527 - 535, 2009.

YEH, C.K. J.; HSU, C. Y.; CHIU, C. H.; HUANG, K. L. **Reaction efficiencies and rate constants for the goethite-catalyzed Fenton-like reaction of NAPL-form aromatic hydrocarbons and chloroethylenes.** Journal of Hazardous Materials, v. 151, p. 562 - 569, 2008.

ZHANG G.; SUN Y.; GAO D.; XU Y.; **Quasi-cube $ZnFe_2O_4$ nanocrystals: Hydrothermal synthesis and photocatalytic activity with TiO_2 (Degussa P25) as nanocomposite**. Materials Research Bulletin, v. 45, p. 755–760, 2010.

ZHANG, X.; DING, Y.; TANG, H.; HAN, X.; ZHU, L.; WANG, N. **Degradation of bisphenol A by hydrogen peroxide activated with CuFeO2 microparticles as a heterogeneous Fenton-like catalyst: Efficiency,stability and mechanism.** Chemical Engineering Journal, v. 236, p. 251–262, 2014.

ZHONG, Y.; LIANG, X.; ZHONG, Y.; ZHU, J.; ZHU, S.; YUAN, P.; HE, H.; ZHANG, J. **Heterogeneous UV/Fenton degradation of TBBPA catalyzed by titanomagnetite: catalyst**

characterization, performance and degradation products. Water Research, v. 46, p. 4633 - 4644, 2012
.

CAPÍTULO 3

RESULTADOS

Neste capítulo estão apresentados os resultados obtidos no decorrer da pesquisa. Três trabalhos desenvolvidos no tema dessa dissertação foram escritos na forma de três artigos, e os mesmos encontram-se conforme o molde das revistas onde foram publicados ou submetidos. Sendo eles:

- Efect of solvent diols on the $ZnFe_2O_4$ synthesis and its use as heterogeneous photo-Fenton catalyst;
- Rapid and facile preparation of zinc ferrite ($ZnFe_2O_4$) oxide by microwave-solvothermal technique and its catalytic activity in heterogeneous photo-Fenton reaction;
- Statistical optimization of Procion Red removal by heterogeneous photo-Fenton reaction using $ZnFe_2O_4$ oxide

3.1 Artigo I : Effect of solvent diols on the $ZnFe_2O_4$ synthesis and its use as heterogeneous photo-Fenton catalyst

Chayene Gonçalves Anchieta [1], Adriano Cancelier [1], Marcio Antonio Mazutti [1], Raquel Cristine Kuhn [1], Andre Gündel [2] and Edson Luiz Foletto [1]

[1] Department of Chemical Engineering, Federal University of Santa Maria, 97105-900, Santa Maria, Brazil; E-Mail: chaya_36@hotmail.com (C.G.A.); adrianocancelier@gmail.com (A.C.); marciomazutti@gmail.com (M.A.M.); raquelckuhn@yahoo.com.br (R.C.K.); efoletto@gmail.com (E.L.F.)
[2] University Campus, Federal University of Pampa, 96413-170, Bagé, Brazil; E-Mail: gundel@gmail.com

O presente artigo foi publicado na revista "Materials", volume 7, páginas de 6281 até 6290, em 3 de setembro de 2014.

DOI:10.3390/ma7096281

Abstract A solvothermal method was used to prepare zinc ferrite spinel oxide ($ZnFe_2O_4$) using ethylene glycol and 1,4 butanediol as solvent diols, and the influence of diols on the physical properties of $ZnFe_2O_4$ particles was investigated. The produced particles were characterized by X-ray powder diffraction (XRD), atomic force microscopy (AFM), Fourier transform infrared spectroscopy (FTIR) and nitrogen adsorption isotherms, and the catalytic activity for the organic pollutant decomposition by heterogeneous photo-Fenton reaction was investigated. Both solvents produced particles with cubic spinel structure. Microporous and mesoporous structures were obtained when ethylene glycol and 1,4 butanediol were used as diols, respectively. A higher pore volume and surface area, as well as a higher catalytic activity for the pollutant degradation were found when 1,4 butanediol was used as solvent.

Keywords: zinc ferrite; $ZnFe_2O_4$; synthesis; solvothermal; photo-Fenton.

1. Introduction

Zinc ferrite ($ZnFe_2O_4$) is a spinel oxide that possesses excellent magnetic and electrical properties [1,2], as well as excellent chemical and thermal stabilities [3]. $ZnFe_2O_4$ oxide has received much attention due to its potential applications in detecting gases [4], adsorbent material for hot-gas desulfurization [5], biomedicine [6], magnetic, optical and electrical behaviors [7-11] and catalytic application [12, 13]. Recently, zinc ferrite has been used as an efficient heterogeneous Fenton catalyst in degrading the organic pollutants from aqueous solution [14-16]. $ZnFe_2O_4$ nanoparticles were developed as catalyst for the degradation of benzotriazole by a heterogeneous photoelectron-Fenton process and have shown to be highly efficient to benzotriazole degradation [16]. A hydrothermal method was used to synthesize $ZnFe_2O_4$ powders with an average size of 10 nm with the aid of sodium oleate, and they presented good photocatalytic activity in the degradation of Rhodamine B dye under the irradiation of simulated solar light [17]. $ZnFe_2O_4$ film fabricated on sulfonated silicon substrate via a novel template-assisted route exhibited good photocatalytic activity in the degradation of Rhodamine B under visible light irradiation [18]. $ZnFe_2O_4$ nanocrystallites were synthesized by microwave sintering and played an important role in degrading the methylene blue dye under visible light [19].

$ZnFe_2O_4$ particles have been prepared using various methods, such as co-precipitation [20,21], sol–gel [22], solid-state reaction [23], glycine combustion method [24], combustion reaction using urea as reducing agent [25,26], hydrothermal synthesis [27], solvothermal and microwave-assisted solvothermal synthesis [28], high energy ball-milling [29], thermal plasma synthesis [30], one-step solid-phase chemical reaction [31], microwave combustion method [32], polyethylene glycol-assisted route [33] and synthesis in supercritical fluids [34,35]. Herein, we report the use of solvothermal route for the preparation of $ZnFe_2O_4$ particles. Solvothermal route offers advantage over the hydrothermal route, because it does not require the use of surfactants or templates in the reaction medium. Solvothermal method was used to fabricate $ZnFe_2O_4$/α-Fe_2O_3 composite hollow nanospheres, including polyethylene glycol as template [36]. Li *et al.* [37] and Kuai *et al.* [38] used ethylene glycol as solvent for the synthesis of $ZnFe_2O_4$ nanospheres and Ce^{3+} doped Zn ferrites, respectively.

Accordingly, this work aimed to synthesize $ZnFe_2O_4$ powders with a solvothermal route, using different solvent diols, and to examine their structural properties. In addition, the catalytic performance for organic dye degradation over $ZnFe_2O_4$ powders was investigated.

2. Experimental Section

2.1. Preparation of powders

The $ZnFe_2O_4$ particles were prepared using the solvothermal method. Zinc nitrate [$Zn(NO_3)_2.6H_2O$, analytical grade] and iron nitrate [$Fe(NO_3)_3.9H_2O$, analytical grade] were used as zinc and iron sources, respectively, without further purification. Stoichiometric amounts of Zn and Fe nitrates (molar ratio Zn:Fe = 1:2) were used for preparing $ZnFe_2O_4$ powders. Two diols were used was solvent, ethylene glycol [$C_2H_4(OH)_2$, analytical grade] and 1,4 butanediol [$C_4H_{10}O_2$, analytical grade]. In a typical synthetic procedure, zinc nitrate (4 mmol) and iron nitrate (8 mmol) were dissolved in 120 mL of ethylene glycol (EG) and mixed with appropriate amount of sodium acetate (CH_3COONa) (60 mmol), under magnetic stirring. Then, the final mixture was charged into a PTFE-lined stainless autoclave, and the solvothermal reaction was carried out at 200 ^oC for 24 h. Subsequently, the autoclave was left to naturally cool off. The solids were filtered, washed with distilled water, and dried at 110 ^oC for 10 h to obtain $ZnFe_2O_4$-EG. A similar procedure to that described above was carried out using 1,4 butanediol (BD) to obtain $ZnFe_2O_4$-DB.

2.2. Characterization of powders

The XRD patterns were obtained on a Rigaku Miniflex 300 diffractometer with a Cu *K*α radiation at 30 kV and 10 mA, with a step size (2θ) of 0.03^o and a count time of 0.9 s per step. The average size of the $ZnFe_2O_4$ spinel crystallite was determined with the Scherrer equation [39]: $D = K.\lambda / (h_{1/2}.\cos\theta)$, where D is the average crystallite size, K the Scherrer constant (0.9), λ the wavelength of incident X-rays (0.1541 nm), $h_{1/2}$ the peak width at half height and θ corresponds to the peak position (in this work, $2\theta = 35.36^o$). The AFM images were obtained by atomic force microscopy (Agilent Technologies 5500 equipment). N_2 adsorption-desorption isotherms measurements were carried out at 77 K using an ASAP 2020 apparatus, at a relative pressure (P/P_0) from 0 to 0.99. FTIR spectra were recorded on a Shimadzu IR-Prestige-21 spectrophotometer in the range of 4000-375 cm^{-1}, using pellets prepared by mixing zinc ferrite powder with KBr powder (10 mg zinc ferrite/300 mg KBr).

2.3. Experimental essays and reaction apparatus

A batch–type reactor was used, consisting of a glass tube (internal diameter of 5.0 cm and 6.0 cm in height) with an economic fluorescent lamp (80 W, emit at wavelength above 400 nm) fixed above the reaction solution. Due to the narrow bandgap of ~1.9 eV [37, 40], $ZnFe_2O_4$ shows a wide absorption in the visible-light region and could be easily excited by visible light, accelerating the degradation of organic molecules from aqueous solution. Visible light assisted Fenton system for the treatment of dyes has been shown to be very promising [41, 42]. The reaction solution was 15 cm apart from the lamp. For the catalytic experiments under visible irradiation, 0.5 g of catalyst was added to 50 mL of Procion Red dye aqueous solution at an initial concentration of 50 mg L^{-1}, followed by adjusting pH to 3.0 by 0.1 M H_2SO_4. Acidic conditions (about pH 3) are required for a better performance of Fenton reaction [41, 43]. Previous to irradiation, the suspension was magnetically stirred in the dark until reaching the adsorption equilibrium. After the adsorption process, an aliquot of hydrogen peroxide (0.04 mol L^{-1}) was added to the solution to initiate the reaction. When H_2O_2 was added, it greatly enhanced the efficiency of degradation, which affects $^{\cdot}OH$ production for the rapid oxidation of contaminants [42, 43]. Then the suspension was irradiated by the lamp, and aliquots were collected at set time intervals using a 5 mL syringe, followed by the filtration of the suspension. The reaction was always kept at room temperature. Dye concentration data were treated in the dimensionless form ($C/C_0 = A/A_0$) and plotted as a function of reaction time, where C_0 represents the absorbance of the initial dye solution and C the absorbance of the dye solution at reaction time t. The absorbance was measured using a UV–vis spectrophotometer (Bel Photonics, SP1105) at maximum wavelength of 543 nm. The concentration of Fe irons leaching from $ZnFe_2O_4$ particles during the reaction process was measured using atomic absorption spectroscopy (Agilent Technologies, 200 series AA).

3. Results and discussion

Fig. 1 shows the XRD patterns of $ZnFe_2O_4$ samples prepared with EG and BD. The diffractograms for both samples indicate that each sample corresponds to a spinel cubic structure according to JCPDS card no. 89-1012. The diffraction peaks at 2θ of 30.05°, 35.36°, 42.78°, 52.96°, 56.78° and 62.2° can be ascribed to the reflection of (220), (311), (400), (422), (511) and (440) planes of the $ZnFe_2O_4$ spinel, respectively. However, a very small amount of ZnO (2θ = 31.7 °) was detected in $ZnFe_2O_4$ synthesized with ethylene glycol, as shown in Fig.

1. The main difference in the X-ray diffractograms of the $ZnFe_2O_4$ samples prepared with EG and BD is the width of the peaks. It may be noted that the $ZnFe_2O_4$-BD sample has wider peaks than those of $ZnFe_2O_4$-EG. This indicates that the $ZnFe_2O_4$-BD sample has smaller average crystallite size. The average crystallite size calculated by Scherrer equation of nanocrystals synthesized with EG was 24.9 nm, while the average crystallite size of nanocrystals produced with BD was 6.0 nm.

Figure 1. XRD patterns of the samples prepared with different solvent diols.

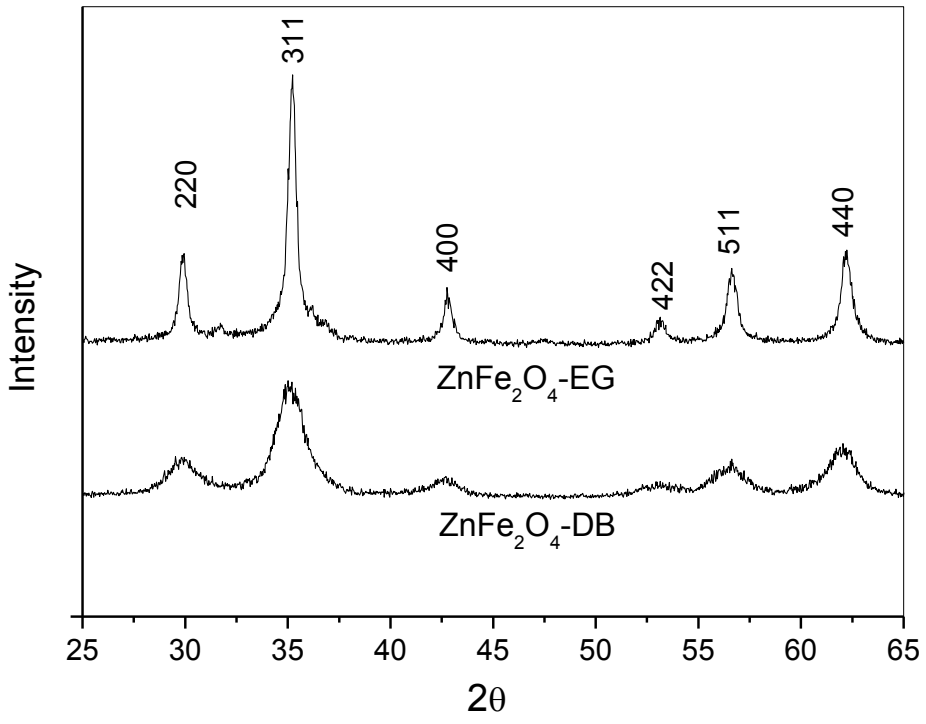

FTIR spectra of the ferrite samples are presented in Fig. 2. The bands at 3440 and 1640 cm^{-1} can be assigned to the stretching vibration mode of adsorbed water molecules on the surface of ferrite crystals [44,45]. However, the main bands that characterize the formation of spinel phase are located at 570 and 440 cm^{-1}, which are associated with the vibrations of Zn-O and Fe-O bonds, respectively [44, 46].

Figure 2. FTIR spectra of the samples prepared with different solvent diols.

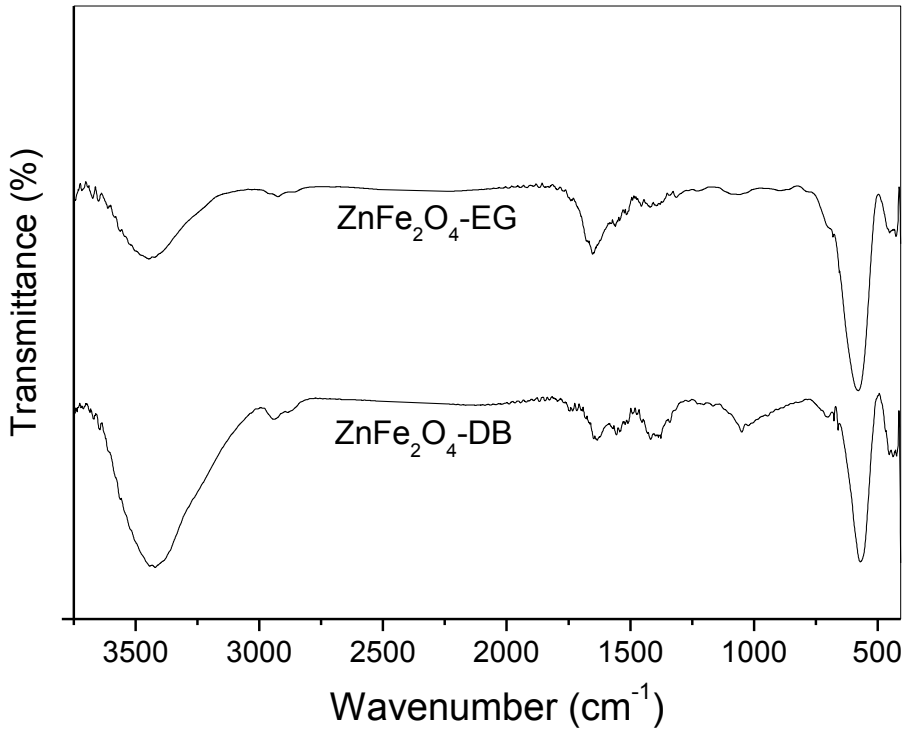

Fig. 3 shows nitrogen adsorption-desorption isotherms (Fig. 3a) of the obtained $ZnFe_2O_4$ samples and their corresponding pore size distribution curves (Fig. 3b). As shown in Fig. 3, the isotherms, as well as the pore size distribution curves of both samples, are significantly different. The nitrogen adsorption-desorption isotherms (Fig. 3a) of the $ZnFe_2O_4$-BD sample are type IV with an H1 hysteresis loop according to the IUPAC classification, which indicates the predominance of mesoporous structure. While those of the $ZnFe_2O_4$-EG sample are of type III, indicating materials with predominantly microporous structure. The size pore distributions (Fig. 3b) of the samples confirm the presence of mesoporous for the $ZnFe_2O_4$-BD sample and microporous for the $ZnFe_2O_4$-EG sample. Pore size distribution consisted of one wide peak centered at 150 Å (15 nm) for the $ZnFe_2O_4$-BD sample. This mesoporosity can be attributed to the interparticle pores due to the crystallites agglomeration. The specific surface area and total pore volume of the $ZnFe_2O_4$-BD sample were 44.6 $m^2\ g^{-1}$ and 0.217 $cm^3\ g^{-1}$ respectively, larger than those of the $ZnFe_2O_4$-EG sample, 14.6 $m^2\ g^{-1}$ and 0.045 $cm^3\ g^{-1}$ respectively. Different values of surface area and pore volume were found when different diols such as ethylene glycol, 1,2 propanediol, 2,3 butanediol and

2-methyl-2,4-pentanediol were used in the preparation of alumina-silica powders using the sol-gel method [47].

Figure 3. (a) N2 adsorption–desorption isotherms measured at 77 K and (b) pore size distribution curves from the adsorption branches through the BJH method.

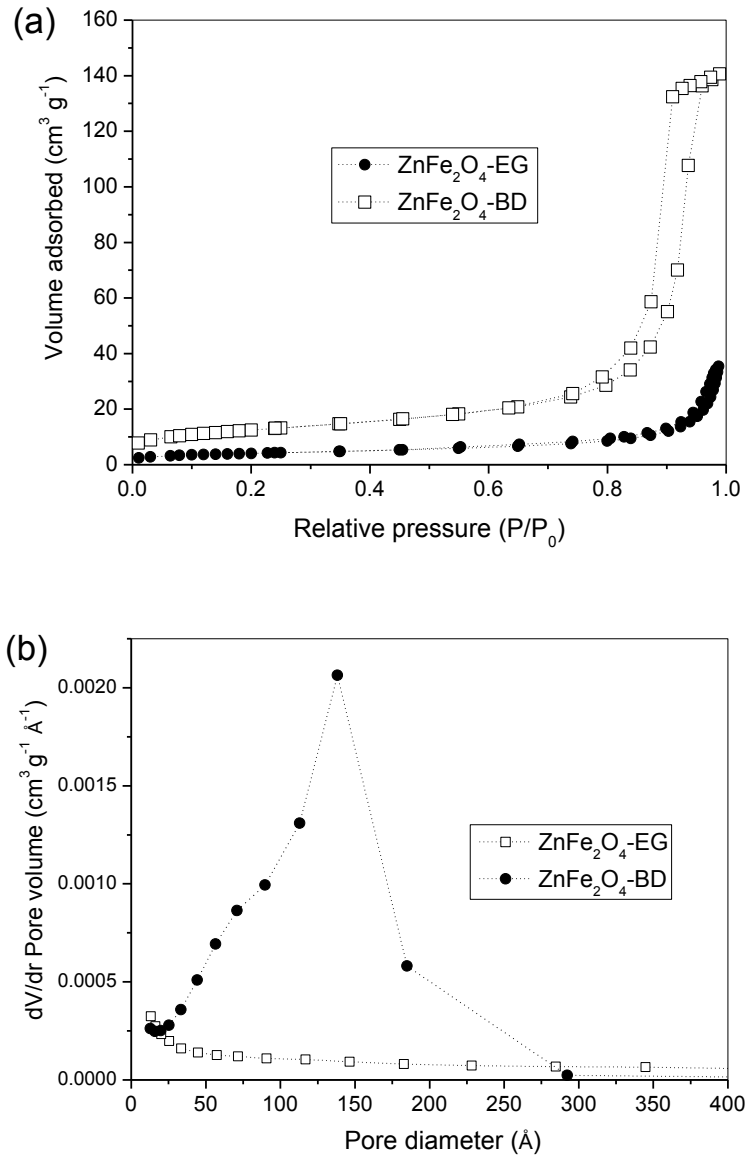

AFM images (Fig. 4) show that the $ZnFe_2O_4$ samples prepared with EG and BD are formed by the agglomeration of small particles that are smaller than 50 nm, which are on the same order of magnitude of those calculated with the Scherrer equation in XRD analysis.

Figure 4. Atomic force microscopy (AFM) of (a) $ZnFe_2O_4$-BD and (b) $ZnFe_2O_4$-EG.

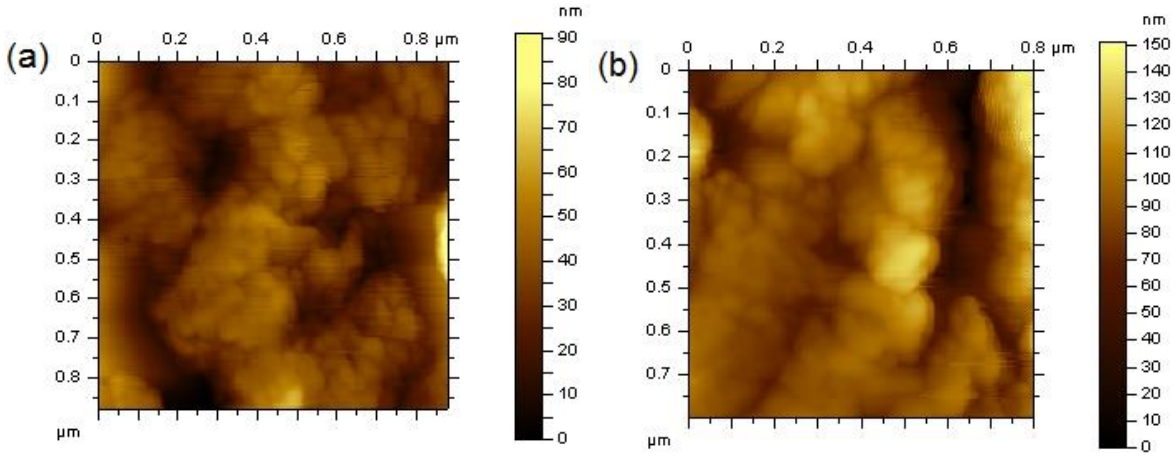

Preliminary experiments were performed in the conditions of photolysis (with presence of visible light irradiation only) and Fenton reaction (with catalyst and hydrogen peroxide in the absence of visible light irradiation), which negligible results (smaller 5 % of dye degradation) were observed for both conditions. In addition, other experiments demonstrated that the dye degradation was negligible when using catalyst in the presence of visible light irradiation and without irradiation. Therefore, the photocatalytic activity of $ZnFe_2O_4$ powders only occurred in the simultaneous presence of visible light irradiation and hydrogen peroxide. Fig. 5 depicts the photocatalytic activity of both $ZnFe_2O_4$ samples in the presence of visible light and hydrogen peroxide. $ZnFe_2O_4$-DB particles showed the highest photocatalytic activity for dye degradation and complete removal occurred at 30 min of irradiation time, while the efficiency of $ZnFe_2O_4$-EG particles reached 85% of dye degradation at 60 min, as shown in Fig. 5a. Thus, it is possible to note that the best catalytic performance occurs in the presence of $ZnFe_2O_4$-DB, and this may be associated with smaller crystallite size and, consequently, higher surface area. Fig. 5b illustrates the reaction kinetics for the dye degradation using both catalysts prepared in this present work. The dye degradation followed the pseudo first-order kinetics [48,49] where the reaction rate constants (k) were obtained from slopes of the fit lines of ln (C/C_0) versus reaction time. The reaction constants values were 29 x 10^{-3} min^{-1} (R^2 = 0.99) and 125 x 10^{-3} min^{-1} (R^2 = 0.99) for the $ZnFe_2O_4$-EG and $ZnFe_2O_4$-BD samples, respectively. Thus, $ZnFe_2O_4$-BD exhibited a rate that was about four times faster than that of $ZnFe_2O_4$-EG, which may associated with its higher surface area. Therefore, the results showed that the $ZnFe_2O_4$-BD sample displayed higher catalytic activity than that of the $ZnFe_2O_4$-EG sample under visible light irradiation. Due to its magnetic property [50], $ZnFe_2O_4$ spinel can be separated and recovered from aqueous solution

through a magnetic field for further reutilization. The leaching of Fe ions in the solution was measured at 60 min irradiation for both catalysts. The concentrations of leached Fe were 4.2 and 4.5 mg L^{-1} for the $ZnFe_2O_4$-BD and $ZnFe_2O_4$-EG catalysts, respectively, which are below the level established by the Brazilian environmental legislation (CONAMA) [51] for discharge in waste effluents, i.e., 15 mg L^{-1}.

Figure 5. (a) Degradation profiles and (b) the variation of ln (C/C_0) of Procion red dye over $ZnFe_2O_4$-EG and $ZnFe_2O_4$-DB. Reaction conditions:initial H_2O_2 concentration = 0.04 mol L-1, catalyst amount = 0.5 g, initial dye concentration =50 mg L–1 and initial pH= 3

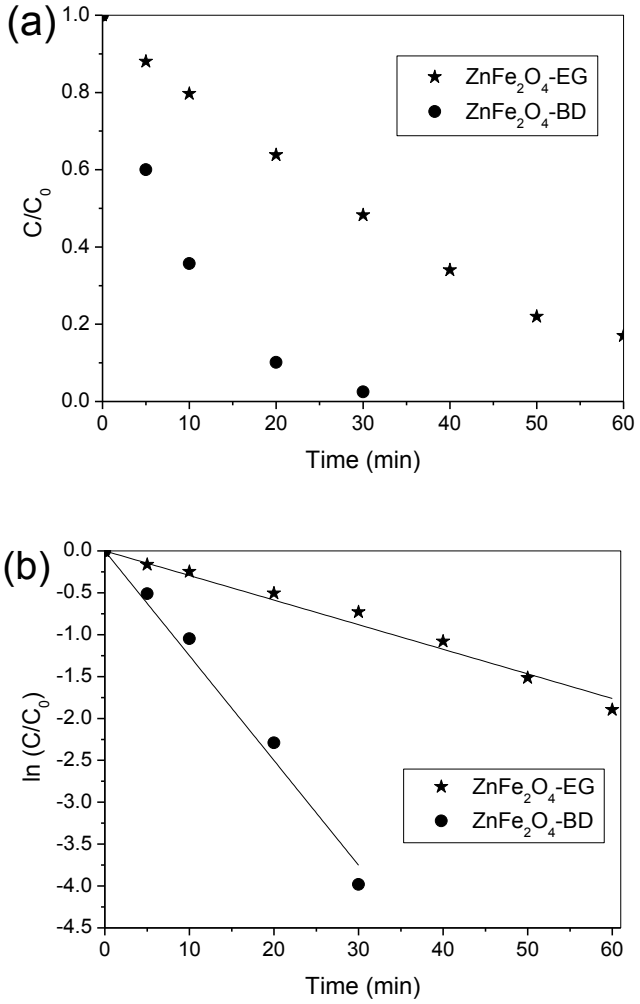

4. Conclusions

A solvothermal technique was used to produce $ZnFe_2O_4$ particles using two diol solvents. Results indicated that different physical properties may be found when different solvents are used for the synthesis of $ZnFe_2O_4$ particles. $ZnFe_2O_4$ particles were used as a heterogeneous photo-Fenton catalyst, exhibiting a good catalytic activity towards the degradation of Procion red dye in the presence of H_2O_2/visible light. Due to its greater surface area, $ZnFe_2O_4$-BD had faster degradation rate compared to that of $ZnFe_2O_4$-EG. The photocatalytic degradation of Procion red dye from aqueous solution in the $ZnFe_2O_4$–visible irradiation-H_2O_2 system followed pseudo first-order kinetics. $ZnFe_2O_4$ catalysts prepared herein presented low iron leaching, and may be easily recovered and separated from aqueous solution with the aid of a magnetic field.

References

1. Mathew, D.S.; Juang, R.S. An overview of the structure and magnetism of spinel ferrite nanoparticles and their synthesis in microemulsions. *Chem. Eng. J.* **2007**, *129*, 51–65.
2. Pradeep, A.; Priyadharsini, P.; Chandrasekaran, G. Structural, magnetic and electrical properties of nanocrystalline zinc ferrite. *J. Alloys Compds.* **2011**, *509*, 3917–3923.
3. Fan, G.; Gu, Z.; Yang, L.; Li, F. Nanocrystalline zinc ferrite photocatalysts formed using the colloid mill and hydrothermal technique. *Chem. Eng. J.* **2009**, *155*, 534–541.
4. Xiangfeng, C.; Xingqin, L.; Guangyao, M. Preparation and gas sensitivity properties of $ZnFe_2O_4$ semiconductors. *Sensors Actuators B: Chem.*. **1999**, *55*, 19–22.
5. Ahmed, M.A.; Alonso, L.; Palacios, J.M.; Cilleruelo, C.; Abanades, J.C. Structural changes in zinc ferrites as regenerable sorbents for hot coal gas desulfurization. *Solid State Ionics*. **2000**, *138*, 51–62.
6. Wan, J.; Jiang, X.; Li, H.; Chen, K. Facile synthesis of zinc ferrite nanoparticles as non-lanthanide T1 MRI contrast agents. *J. Mater. Chem.* **2012**, *22*, 13500–13505.
7. Albuquerque, A.S.; Ardisson, J.D.; Bittencourt, E.; Macedo, W.A.A. Structure and magnetic properties of granular NiZn-ferrite-SiO_2. *Mater. Res.* **1999**, *2*, 235–238.
8. Kumar, G.S.Y.; Naik, H.S.B.; Roy, A.S.; Harish, K.N.; Viswanath, R. Synthesis, optical and electrical properties of $ZnFe_2O_4$ nanocomposites. *Nanotechn. Nanomater.* **2012**, *2*, DOI: 10.5772/56169.
9. Mekap, A.; Das, P.R.; Choudhary, R.N.P. Dielectric, magnetic and electrical properties of $ZnFe_2O_4$ ceramics. *J. Mater. Sci.: Mater. Electronics.* **2013**, *24*, 4757–4763.
10. Gama, A.M.; Rezende, M.C. Complex permeability and permittivity variation of radar absorbing materials based on MnZn ferrite in microwave frequencies. *Mater. Res.* **2013**, *16*, 997–1001.

11. Yelenich, O.V.; Solopan, S.O.; Kolodiazhnyi, T.V.; Dzyublyuk, V.V.; Tovstolytkin, A.I.; Belous, A.G. Magnetic properties and high heating efficiency of $ZnFe_2O_4$ nanoparticles. *Mater. Chem. Phys.* **2014**, *146*, 129–135.
12. Toledo-Antonio, J.A.; Nava, N.; Martinez, M.; Bokhimi, X. Correlation between the magnetism of non-stoichiometric zinc ferrites and their catalytic activity for oxidative dehydrogenation of 1-butene. Appl. Catal. A: Gen. **2002**, *234*, 137–144.
13. Casbeer, E.; Sharma, V.K.; Li, X.Z. Synthesis and photocatalytic activity of ferrites under visible light: A review. *Sep. Purif. Technol.* **2012**, *87*, 1–14.
14. Liu, L.; Zhang, G.; Wang, L.; Huang, T.; Qin, L. Highly active S-modified $ZnFe_2O_4$ heterogeneous catalyst and its photo-Fenton behavior under UV–visible irradiation. *Ind. Eng. Chem. Res.* **2011**, *50*, 7219–7227.
15. Li, P.; Xu, H.Y.; Li, X.; Liu, W.C.; Li, Y. Preparation and evaluation of a photo-Fenton heterogeneous catalyst: spinel-typed $ZnFe_2O_4$. *Adv. Mater. Res.* **2012**, *550–553*, 329–335.
16. Wu, J.; Pu, W.; Yang, C.; Zhang, M.; Zhang, J. Removal of benzotriazole by heterogeneous photoelectro-Fenton like process using $ZnFe_2O_4$ nanoparticles as catalyst. *J. Environm. Sci.* **2013**, *25*,801–807.
17. Sun, Y.; Wang, W.; Zhang, L.; Sun, S.; Gao, E. Magnetic $ZnFe_2O_4$ octahedra: Synthesis and visible light induced photocatalytic activities. *Mater. Lett.* **2013**, *98*, 124–127.
18. Nan, C.; Fan, G.; Fan, J.; Li, F. Template-assisted route to porous zinc ferrite film with enhanced visible-light induced photocatalytic performance. *Mater. Lett*. **2013**, *106*, 5–7.
19. Dom, R.; Subasri, R.; Radha, K.; Borse, P.H. Synthesis of solar active nanocrystalline ferrite, MFe_2O_4 (M: Ca, Zn, Mg) photocatalyst by microwave irradiation. *Solid State Communic.* **2011**, *151*, 470–473.
20. Teixeira, A.M.R.F.; Ogasawara, T.; Nóbrega, M.C.S. Investigation of sintered cobalt-zinc ferrite synthesized by coprecipitation at different temperatures: a relation between microstructure and hysteresis curves. *Mater. Res*. **2006**, *9*, 257–262.
21. Li, Q.; Bo, C.; Wang, W. Preparation and magnetic properties of $ZnFe_2O_4$ nanofibers by coprecipitation–air oxidation method. *Mater. Chem. Phys*. **2010**, *124*, 891–893.
22. Liu, H.; Guo, Y.; Zhang, Y.; Wu, F.; Liu, Y.; Zhang, D. Synthesis and properties of ZnFe2O4 replica with biological hierarchical structure. *Mater. Sci. Eng.: B*, **2013**, *178*, 1057-1061.
23. Jesus, C.B.R.; Mendonça, E.C.; Silva, L.S.; Folly, W.S.D.; Meneses, C.T.; Duque, J.G.S. Weak ferromagnetic component on the bulk $ZnFe_2O_4$ compound. *J. Magnetism Magnetic Mater*. **2014**, *350*, 47–49.
24. Patil, J.Y.; Nadargi, D.Y.; Gurav, J.L.; Mulla, I.S.; Suryavanshi, S.S. Glycine combusted $ZnFe_2O_4$ gas sensor: Evaluation of structural, morphological and gas response properties. *Ceram. Inter*. **2014**, *40*, 10607–10613.
25. Costa, A.C.F.M; Tortella, E.; Neto, E.F.; Morelli, M.R.; Kiminami, R.H.G.A. Sintering of Ni-Zn ferrite nanopowders by the constant heating rate (CHR) method. *Mater. Res*. **2004**, *7*, 523–528.
26. Dantas, J.; Santos J.R.D.; Cunha, R.B.L.; Kiminami, R.H.G.A.; Costa, A.C.F.M. Use of Ni-Zn ferrites doped with Cu as catalyst in the transesterification of soybean oil to methyl esters. Mater. Res. **2013**, *16*, 625–627.
27. Han, L.; Zhou, X.; Wan, L.; Deng, Y.; Zhan, S. Synthesis of $ZnFe_2O_4$ nanoplates by succinic acid-assisted hydrothermal route and their photocatalytic degradation of rhodamine B under visible light. *J. Environm. Chem. Eng.* **2014**, *2*, 123–130.
28. Blanco-Gutierrez, V.; Climent-Pascual, E.; Torralvo-Fernandez, M.J.; Saez-Puche, R.; Fernandez-Diaz, M.T. Neutron diffraction study and superparamagnetic behavior of

$ZnFe_2O_4$ nanoparticles obtained with different conditions. *J. Solid State Chem.* **2011**, *184*,1608–1613.

29. Banerjee, A.; Bid, S.; Dutta, H.; Chaudhuri, S.; Das, D.; Pradhan, S.K. Microstructural changes and effect of variation of lattice strain on positron annihilation lifetime parameters of zinc ferrite nanocomposites prepared by high enegy ball-milling. *Mater. Res.* **2012**, *15*, 1022–128.
30. Mohai, I.; Szépvölgyi, J.; Bertóti, I.; Mohai, M.; Gubicza, J.; Ungár, T. Thermal plasma synthesis of zinc ferrite nanopowders. *Solid State Ionics*. **2001**, *141–142*, 163–168.
31. Cao, Y.; Jia, D.; Hu, P.; Wang, R. One-step room-temperature solid-phase synthesis of $ZnFe_2O_4$ nanomaterials and its excellent gas-sensing property. *Ceram. Inter.* **2013**, *39*, 2989-2994.
32. Manikandan, A.; Kennedy, L.J.; Bououdina, M.; Vijaya, J.J. Synthesis, optical and magnetic properties of pure and Co-doped $ZnFe_2O_4$ nanoparticles by microwave combustion method. *J. Magnetism Magnetic Mater*. **2014**, *349*, 249-258.
33. Köseoğlu, Y.; Baykal, A.; Toprak, M.S.; Gözüak, F.; Başaran, A.C.; Aktaş, B. Synthesis and characterization of $ZnFe_2O_4$ magnetic nanoparticles via a PEG-assisted route. *J. Alloys Compnds*. **2008**, *462*, 209–213.
34. Oliver, S.A. Localized spin canting in partially inverted $ZnFe_2O_4$ fine powders. *Phys. Review B.* **1999**, *60*, 3400-3405.
35. Cabañas, A.; Poliakoff, M. The continuous hydrothermal synthesis of nano-particulate ferrites in near critical and supercritical water. *J. Mater. Chem*. **2001**, *11*, 1408–1416.
36. Shen, Y.; Li, X.; Zhao, Q.; Hou, Y.; Tade, M.; Liu, S. Facile synthesis and characterization of $ZnFe_2O_4$/α-Fe_2O_3 composite hollow nanospheres. *Mater. Res. Bull*. **2011**, *46*, 2235–2239.
37. Li, X.; Hou, Y.; Zhao, Q.; Wang, L. A general, one-step and template-free synthesis of sphere-like zinc ferrite nanostructures with enhanced photocatalytic activity for dye degradation. *J. Coll. Interf. Sci.* **2011**, *358*, 102-108.
38. Kuai, S.; Zhang, Z.; Nan, Z. Synthesis of Ce^{3+} doped $ZnFe_2O_4$ self- assembled clusters and adsorption of chromium(VI). *J. Hazard. Mater.* **2013**, *250–251*, 229–237.
39. Cullity, B.D.; Stock, S.R. *Elements of X-Ray Diffraction*, 3rd Ed., Prentice-Hall Inc., New Jersey, 2001.
40. Köseoğlu, Y.; Baykal, A.; Gözüak, F.; Kavas, H. Structural and magnetic properties of $Co_xZn_{1-x}Fe_2O_4$ nanocrystals synthesized by microwave method. *Polyhedron*. **2009**, *28*, 2887-2892.
41. Hou, Y.; Li, X.; Zhao, Q.; Chen, G. $ZnFe_2O_4$ multi-porous microbricks/graphene hybrid photocatalyst:Facile synthesis, improved activity and photocatalytic mechanism. *Appl. Catal. B: Environm.*. **2013**, *142– 143*, 80– 88.
42. Han, L.; Zhou, X.; Wan, L.; Deng, Y.; Zhan, S. Synthesis of $ZnFe_2O_4$ nanoplates by succinic acid-assisted hydrothermal route and their photocatalytic degradation of rhodamine B under visible light. *J. Environm. Chem. Eng.* **2014**, *2*,n123–130.
43. Mizukami, F.; Kiyozumi, Y.; Sano, T.; Niwa, S.I.; Toba, M.; Shin, S. Effect of solvent diols and ligands on the properties of sol-gel alumina-silicas. *J. Sol-Gel Sci. Technol*. **1998**, *13*, 1027–1031.

44. Borhan, A.I.; Samoila, P.; Hulea, V.; Iordan, A.R.; Palamaru, M.N. Effect of Al^{3+} substituted zinc ferrite on photocatalytic degradation of orange I azo dye. *J. Photochem. Photobiol. A: Chem.* **2014**, *279*, 17–23.
45. Anchieta, C.G.; Sallet, D.; Foletto, E.L.; Silva, S.S.; Chiavone-Filho, O.; Nascimento, C.A.O. Synthesis of ternary zinc spinel oxides and their application in the photodegradation of organic pollutant. *Ceram. Inter.* **2014**, *40*, 4173–4178.
46. National Council on Environmental (Brazil). Available online: http://www.mma.gov.br/port/conama (accessed on 06 july 2014).

3.2 Artigo II: Rapid and facile preparation of zinc ferrite ($ZnFe_2O_4$) oxide by microwave-solvothermal technique and its catalytic activity in heterogeneous photo-Fenton reaction

Chayene G. Anchieta[1], Eric C. Severo[1], Caroline Rigo[1], Marcio A. Mazutti[1], Raquel C. Kuhn[1], Edson I. Muller[2], Erico M. M. Flores[2], Regina F. P. M. Moreira[3], Edson L. Foletto[1]

[1] Department of Chemical Engineering, Federal University of Santa Maria, 97105-900, Santa Maria, Brazil
[2] Department of Chemistry, Federal University of Santa Maria, 97105-900, Santa Maria, Brazil
[3] Department of Chemical Engineering and Food Engineering, Federal University of Santa Catarina, 88040-970, Florianópolis, Brazil

O presente artigo foi submetido para a revista "Materials Chemistry and Physics". O artigo está sob avaliação dos revisores.

Abstract. In this work zinc ferrite ($ZnFe_2O_4$) oxide was rapidly and easily prepared by microwave-solvothermal route and its catalytic property in photo-Fenton reaction was evaluated. The effects of microwave heating time and power on the properties of produced particles were investigated. X-ray diffraction (XRD), Fourier transform infrared spectroscopy (FTIR), atomic force microscopy (AFM) and nitrogen adsorption-desorption isotherms were the techniques used for characterizing the solid products. The synthesized material was tested as a catalyst in the degradation of the textile dye molecule by the heterogeneous photo-Fenton process. Characterization results showed that the microwave heating time and power have significant influences on the formation of the phase spinel as well as on its physical properties. The reaction results showed that the $ZnFe_2O_4$ oxide has good photocatalytic activity, which can be attributed to high surface area and pore volume, and large pore size. The $ZnFe_2O_4$ oxide produced by the microwave irradiation exhibited promising photocatalytic activity for the removal of textile dye, reaching nearly 100% of decolorization at 40 min and 60 % of mineralization at 240 min. Therefore, $ZnFe_2O_4$ particles rapidly prepared by the microwave route have the potential for use in treatment of textile wastewater by the heterogeneous photo-Fenton process.

Keywords: Zinc ferrite, synthesis, microwave heating, catalyst, photo-Fenton

Introduction

Zinc ferrite is spinel oxide that has a cubic structure and great potential in various technology applications such as gas sensors [1], magnetic and superparamagnetic materials [2,3], adsorbents [4], materials with optical and dielectric properties [5,6], antibacterial agent [7], catalysts [8] and photocatalysts [9]. Dyeing industries such as textiles and tanneries generate dye containing effluents, which are toxic and need to be subjected to treatment. Recently, advanced oxidation processes (AOPs) have been widely applied to degrade organic pollutants from aqueous solution. Among the AOPs, the heterogeneous Fenton reaction is one of the most interest processes, which use iron based catalysts and the major advantage is their easy recovery after the treatment process. However, few studies have been reported in the literature regarding the use of zinc ferrite for degradating the organic pollutants by the heterogeneous Fenton process under visible light irradiation have been reported in the literature [10-14]. Compared with ultraviolet light, visible light presents significant advantages in irradiation safety, low cost of lamp and smaller electrical energy consumption. Herein, $ZnFe_2O_4$ powders were synthesized by the microwave-solvothermal route and their catalytic properties on the degradation of an organic pollutant (industrial textile dye) under visible light were evaluated.

Preparation of zinc ferrite oxide with desired physical properties for application in several research fields has become an essential focus in recent years. Thus $ZnFe_2O_4$ ternary oxide has been synthesized by several methods such as precipitation followed by calcination [2], succinic acid-assisted hydrothermal route [13], electrospinning [15], surfactant-assisted hydrothermal synthesis [16], sol–gel method followed by calcination[17], glycine combustion [18], solvothermal synthesis [19,20], sol–gel auto combustion reaction [21], polyethylene glycol-assisted route [22], hydrothermal method with the presence of sodium oleate [23], one-step solid-phase chemical reaction [24], mechanical ball milling [25], solid-state reaction [26] and microwave route [27]. In recent years, route using microwave irradiation has received great attention due to some advantages such as simplicity and rapidness of the synthesis process, homogeneity, higher yield, better reproducibility and energy-saving [27-33]. $ZnFe_2O_4$ nanoparticles were synthesized by the microwave combustion method using urea as the fuel and their optical and magnetic properties were investigated [28]. Microwave-hydrothermal ionic liquid synthesis and photocatalytic property over phenol of $ZnFe_2O_4$ nanoparticles were studied [29]. A magnetic $ZnFe_2O_4$ was synthesized by microwave assisted hydrothermal method and used as an adsorbent for the removal of acid

dye Acid Red 88 (AR88) from aqueous solution [30]. $ZnFe_2O_4$ nanoparticles with supermagnetic property have been obtained by microwave-assisted solvothermal route [31]. A photocatalyst of spinel $ZnFe_2O_4$ oxide was synthesized (at low temperature ~ 973 K) by microwave heating, in one sixtieth of the time required for that of the conventional method [32]. Microwave combustion with glycine as fuel has been used to synthesize zinc ferrite particles, and their magnetic properties were investigated [33]. Herein, with respect to synthesis route, the present contribution relates the use of ethylene glycol as a solvent to prepare $ZnFe_2O_4$ particles in a microwave assisted solvothermal process, where the roles of factors as microwave heating power and time were studied and the optimal conditions for synthesis of well crystalized porous $ZnFe_2O_4$ were evaluated.

In this context, $ZnFe_2O_4$ oxide was prepared by the use of microwave irradiation as energy source using ethylene glycol as a solvent. Microwave heating time and power were the synthesis parameters investigated on the formation of $ZnFe_2O_4$ phase. In addition, this material was used in the heterogeneous photo-Fenton reaction in order to evaluate its catalytic activity on the decolorization and mineralization of organic dye under visible light.

Experimental

2.1. Preparation and characterization of material

$ZnFe_2O_4$ particles were prepared by solvothermal method using microwave energy. Zinc nitrate [$Zn(NO_3)_2.6H_2O$, analytical grade] and iron nitrate [$Fe(NO_3)_3.9H_2O$, analytical grade] were used as zinc and iron sources, respectively. Ethylene glycol [$C_2H_4(OH)_2$, analytical grade] was used as a solvent. In a typical synthetic procedure, stoichiometric amounts of Zn and Fe nitrates (molar ratio Zn:Fe = 1:2) were used for preparing the spinel. Zinc nitrate (4 mmol) and iron nitrate (8 mmol) were dissolved in 120 mL of ethylene glycol and mixed with an appropriate amount of sodium acetate (CH_3COONa) (60 mmol), under magnetic stirring. The mixture was charged into a quartz vessel and transferred to a microwave oven (Multiwave 3000 microwave sample preparation system, Anton Paar, Graz, Austria). The internal volume of quartz vessels was 80 mL and the maximum operational temperature and pressure were set at 250 °C and 60 bar, respectively. Operational procedure for using the microwave equipment was similar to the one described in previous works by our research group [34, 35]. Firstly, an optimum heating time at a constant microwave power (initially chosen as 1000 W) was investigated. The microwave-heating program was started

by applying (i) 1000 W with a ramp of 5 min, (ii) 1000 W for 5 min, and (iii) 0 W for 20 min (cooling step). The procedures (i and iii) were the same for the reaction times of (ii) 10, 20 and 30 min. Secondly, different microwave powers at the optimum time (10 min) were investigated. Then the procedure (i and ii) was taken at 600W, 700W, 800W and 900W for (ii) 10 min. The synthesized solids in both procedures were filtered, washed with distilled and absolute ethanol, and dried at 110 ^{o}C for 10 h.

$ZnFe_2O_4$ particles were characterized by X-ray diffraction (XRD), infrared spectroscopy (FTIR) and BET surface area measurements. X-ray diffraction patterns were obtained using a Rigaku Miniflex 300 diffractometer. The X-ray source was Cu-Kα radiation, powered at 30 kV and 10 mA. Data were collected over the 2θ range 20–65º with a step size of 0.03º and a count time of 0.9 s per step. The average crystallite size was determined using the Scherrer equation (Eq.1) [36]:

$$D = \frac{K \,.\, \lambda}{h_{1/2} \,.\, \cos\theta} \quad (1)$$

where D is the average crystallite size, K is the Scherrer constant (0.90), λ is the wavelength of the X-ray radiation (0.1541 nm for Cu-Kα), $h_{1/2}$ is the peak width at half height and θ corresponds to the peak position (in the current study, 2θ = 35.36^{o}). By means of infrared spectroscopy, FTIR spectra of all samples pressed into KBr pellets (10 mg zinc ferrite/300 mg KBr) were recorded by a Shimadzu IR-Prestige-21 spectrometer. IR spectra were measured in the range 4000-375 cm^{-1}. The BET surface area and pore size distribution were obtained from nitrogen adsorption-desorption isotherms measurements at 77 K, carried out on an ASAP 2020 apparatus at relative pressure (P/P_o) ranging from 0 to 0.99.

2.2. Reaction apparatus, experimental essay and analytical procedures

The photo-Fenton experiment was performed in a batch–type reactor, consisting of a 100 mL glass tube (internal diameter of 5.0 cm and 6.0 cm in height) with an economical fluorescent lamp (80 W, Philips, luminous efficacy of irradiation = 65 lumens/W, emission at wavelength above 400 nm), fixed 10 cm above the reaction solution. The reactor was covered with a polycarbonate protective film to cut any percentage of UV light emitted by the lamp. However, an experimental test was carried out without polycarbonate film and no difference was observed on the degradation result. For the reaction experiment, 0.025 g of catalyst was added to 50 mL of Procion Red dye aqueous solution (Procion Red dye is extensively used in the textile industry; *CI* Reactive Red 141; CAS number 61931-52-0; chemical formula is $C_{52}H_{34}O_{26}S_8Cl_{12}N_{14}$; molecular weight = 1,952 g mol^{-1}; chemical structure is shown in a

previous study [37]) at an initial concentration of 65 mg L^{-1}, followed by adjusting pH to 2.0 by 0.1 M H_2SO_4. It is known that the acidic condition (pH around 3) is required for a promising performance of the Fenton reaction [38, 39].

Before irradiation, the suspension was magnetically stirred in the dark until the adsorption equilibrium was reached. After the adsorption process, an aliquot of hydrogen peroxide (H_2O_2) (0.1 mL with concentration 10 mol L^{-1}) was added to the solution to initiate the reaction. Addition of H_2O_2 into reaction solution improves the performance of pollutant degradation because it generates more $^{\bullet}OH$ radicals, resulting in rapid oxidation of contaminants [39, 40]. Then the suspension was irradiated by the lamp, and aliquots were collected at set time intervals, followed by suspension filtration (PVDF membrane). Experiments were carried out at room temperature. The decolorization efficiency of the dye was treated in the dimensionless form (C/C_0) and plotted as a function of reaction time, where C_0 is the initial concentration of dye and C is the concentration of dye at reaction time t. The concentration was determined by absorbance reading on an UV–vis spectrophotometer (Bel Photonics, SP1105) at a maximum wavelength of 543 nm. Mineralization was monitored in terms of total organic carbon (TOC) measurements on a *TOC-L CPH*/*CPN* analyzer (Shimadzu). The mineralization efficiency of the dye was treated in the dimensionless form (TOC/TOC_0) and plotted as a function of reaction time, where TOC is the initial total organic carbon concentration and TOC_0 is the concentration at reaction time t. The concentration of iron leaching from $ZnFe_2O_4$ particles during the reaction process was measured by atomic absorption spectroscopy (Agilent Technologies, 200 series AA). For detecting the presence of any residual H_2O_2 in the end of reaction, MQuant peroxide test strips were used.

Results and discussion

XRD (Fig. 1) was used to investigate the phase of produced $ZnFe_2O_4$ oxide. Fig. 1a shows XRD diffractograms of samples prepared at 5, 10, 20 and 30 min for microwave power of 1000W, whereas Fig.1b presents XRD patterns of samples prepared for 10 min at different microwave powers (600, 700, 800 and 900 W). In Fig. 1a, the diffractograms of the samples prepared above 10 min indicate a monophasic spinel cubic structure according to JCPDS card no. 89-1012, whereas below 10 min the formation of oxide spinel did not occur. Yet for the samples prepared for 10 min at different microwave powers (Fig. 2b), the formation of phase spinel only occurs for powers above 700 W. These findings demonstrate that the parameters

time and power significantly influence the synthesis process of the $ZnFe_2O_4$ spinel. The diffraction peaks at 2θ of 30.05^o, 35.36^o, 36.77^o 42.78^o, 52.96^o, 56.78^o and 62.2^o can be ascribed to the reflection of (220), (311), (222), (400), (422), (511) and (440) planes of the $ZnFe_2O_4$ spinel, respectively. No impurity peaks are observed, indicating that the samples obtained via microwave method consist of single phases. Crystallite size obtained by the Scherrer equation from XRD results for all $ZnFe_2O_4$ samples is shown in Table 1. For all samples, the crystallite size was of 155-252 Å, and it is slightly smaller for the samples prepared at highest power, 1000 W

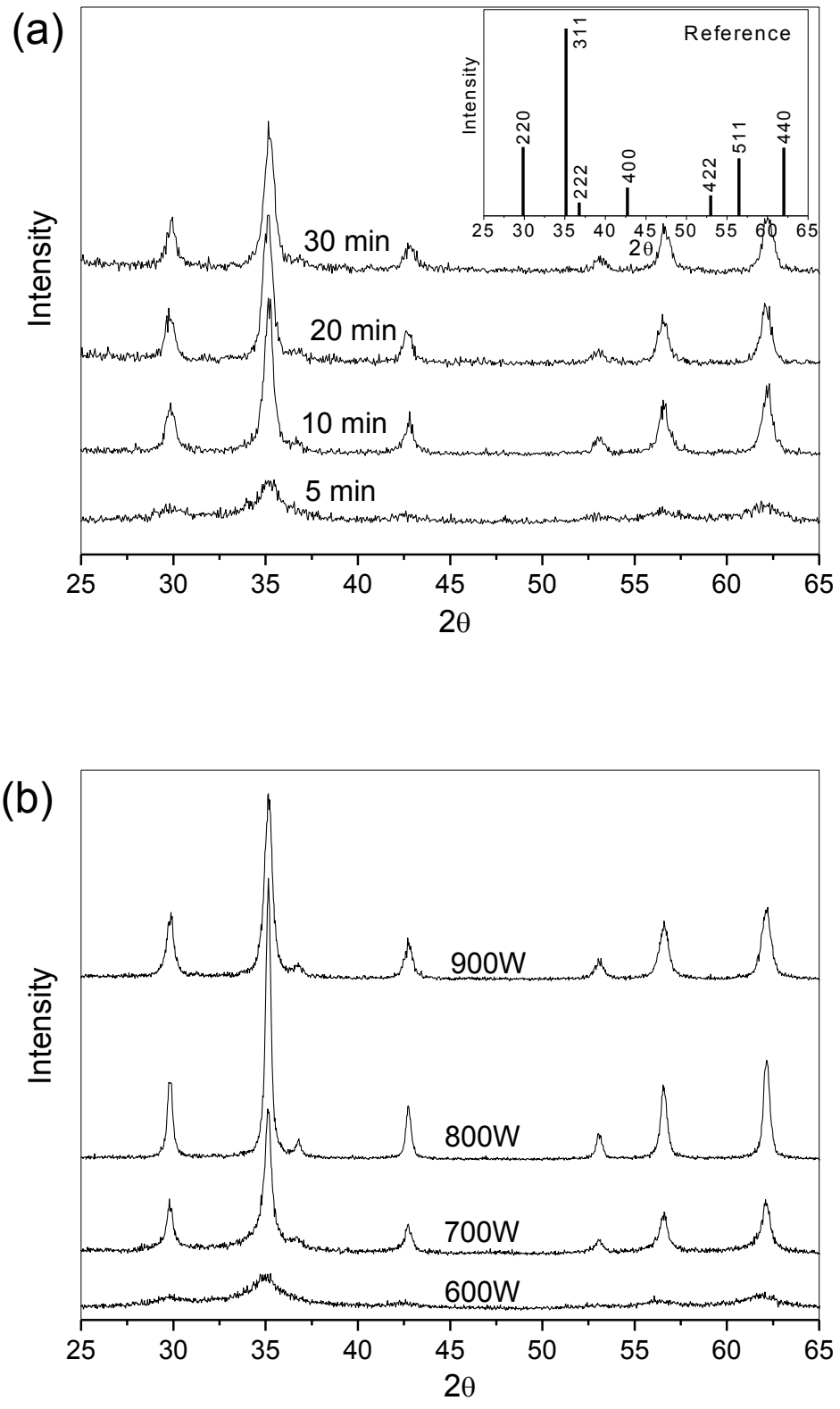

Fig. 1. XRD patterns of samples prepared (a) at 1000W at different times, and (b) for 10 min at different microwave powers. Inset at figure a: $ZnFe_2O_4$ reference according to JCPDS card no. 89-1012.

Nitrogen adsorption-desorption isotherms of $ZnFe_2O_4$ samples and their pore size distribution curves are shown in Fig. 3. The corresponding parameters including BET surface area, total pore volume and average pore size are listed in Table 1. Fig. 3a shows that all samples presented similar behavior, and can be categorized as type III with H_3 hysteresis loop. The H_3 hysteresis type is characteristic of pores with non-uniform size formed from aggregated or agglomerated particles [41]. The pore size distribution curves (Fig. 3b) display a wide distribution, with predominance in the mesoporous region (20 Å < pore size < 500 Å). From Table 1, the average pore size for all samples is located in this region. This characteristic mesoporous structure may be attributed to a variety of accumulated pore voids between agglomerations of particles.

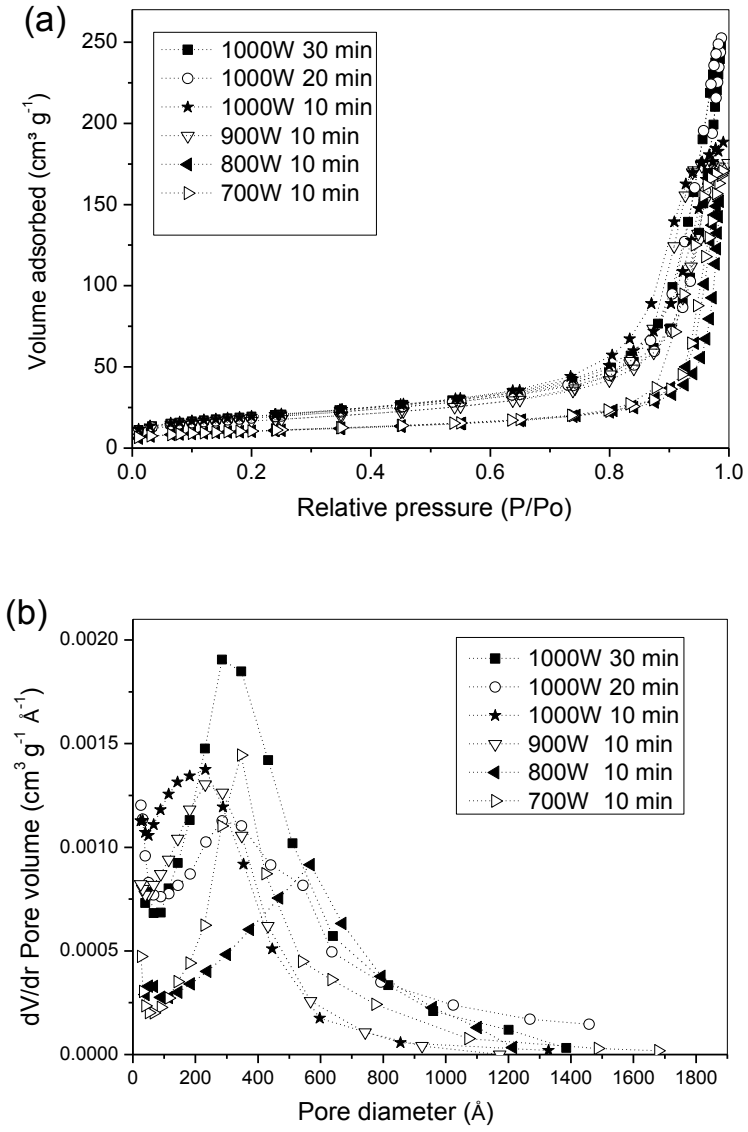

Fig. 2. (a) N2 adsorption-desorption isotherms measured at 77 K and (b) pore size distribution curves from the adsorption isotherm of the different samples.

Table 1. Physical parameters of $ZnFe_2O_4$ particles synthesized at different times and microwave powers.

Sample	Crystallite size (Å)	Surface area ($m^2\ g^{-1}$)	Total pore volume ($cm^3\ g^{-1}$)	Average pore size (Å)
1000 W 30 min	160	70	0.386	215
1000 W 20 min	155	68	0.390	209
1000 W 10 min	177	70	0.301	165
900 W 10 min	195	60	0.271	181
800W 10 min	252	36	0.189	205
700 W 10 min	236	38	0.252	266

It is well known that the properties of catalysts are sensitively related to their porous structure. These physical characteristics favor the contact between the pollutant molecules and catalyst surface, positively influencing on the efficiency of the catalyst. In this work (see Table 1), higher values of surface area (70 $m^2\ g^{-1}$), pore volume (0.390 $cm^3\ g^{-1}$) and pore size (215 Å) were obtained at highest microwave power (1000 W). Thus this favorable pore structure is an essential characteristic for catalytic purpose. For comparison purposes, pore structure parameters of $ZnFe_2O_4$ powders prepared by different methods found in literature are shown in Table 2. From Table 2, it can be seen that each method results in $ZnFe_2O_4$ particles with different pore characteristics. Therefore, the preparation method strongly affects their pore structures.

Table 2 Pore structure parameters of crystalline $ZnFe_2O_4$ powders prepared by different methods found in literature.

Synthesis route	Surface area ($m^2\ g^{-1}$)	Average pore size (Å)	Total pore volume ($cm^3\ g^{-1}$)	References
Microwave-solvothermal	37-70	177-215	0.190-0.390	Present work
Succinic acid-assisted hydrothermal	61-95	9-180	0.092	[13]
Solvothermal	14.6-44.6	< 150	0.045-0.217	[14]
Solvothermal	51.81	77.9	-	[19]
Microwave	6	-	-	[32]
Microwave-assisted combustion	3.5	-	-	[33]
Co-preciptation	16-58	44-92	0.240-0.260	[42]
High-energy ball milling	37	75.35	0.070	[43]
Co-precipitation	45.4	-	-	[44]
Combustion method	45.95	-	-	[45]
Sol-gel auto-combustion	36	-	-	[46]
Mechanochemical	12.3	-	-	[47]
One-pot route	11.51	-	-	[48]
Sol–gel	8	-	-	[49]
Pechini process	4.6-12	-	-	[50]
Sol-gel-self-combustion	22.2	-	-	[51]
Sol–gel auto-combustion	8	-	-	[52]
Self-combustion	3	-	0.004	[53]
Polymerized complex	2-18	-	-	[54]
Solid state reaction	1-4	-	-	[54]

FTIR analysis provides some structural and surface information regarding the material prepared. Fig. 3 shows the FTIR spectra of $ZnFe_2O_4$ samples. The vibrational spectra were emitted in the bands at the values 420, 570, 1050, 1380, 1630, 2925, 3450 cm^{-1}. Spectra around of 570 cm^{-1} are attributed to intrinsic vibrations about tetrahedral complexes and around of 420 cm^{-1} to octahedral complexes [55]. The presence of the small band at 420 cm^{-1} can be attributed to octahedral bonding of Fe-O and at 570 cm^{-1}, it is related to tetrahedral bonding of Zn-O, which are characteristics of spinel phase formation of $ZnFe_2O_4$ [56]. Bands at 1050 cm^{-1} and between 1600 and 3800 cm^{-1} are associated with the presence of humidity absorbed on the $ZnFe_2O_4$ sample [57]. The small bands that appear at 1381cm^{-1} can be attributed to metal-O-H bending of surface groups.

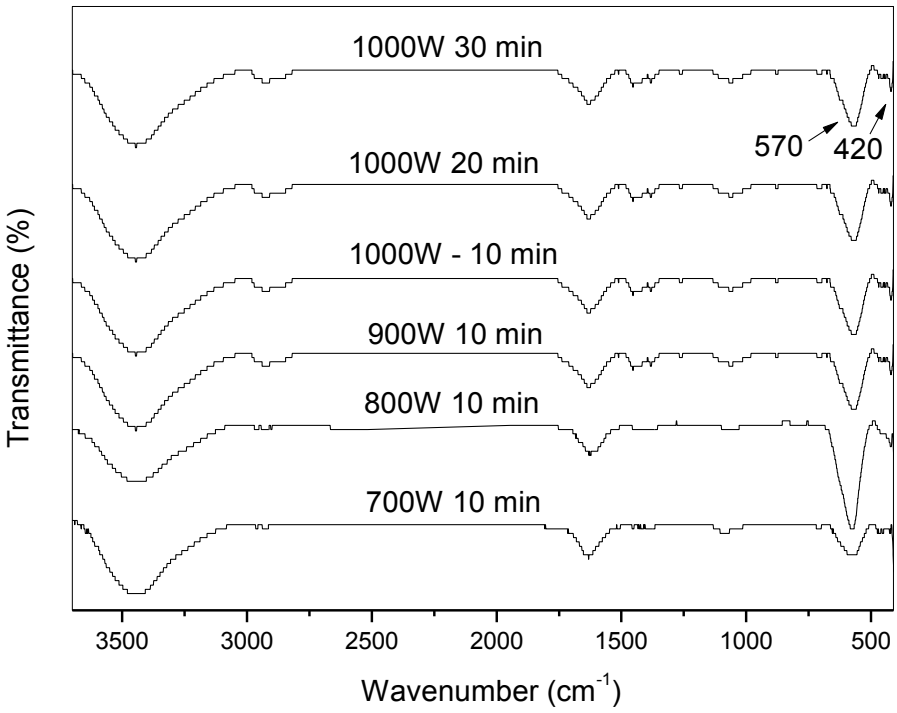

Fig. 3. FTIR spectra of $ZnFe_2O_4$ samples.

Catalytic activity of $ZnFe_2O_4$ samples was evaluated by performing experiments on the decolorization and mineralization of dye from aqueous solution (Fig. 4). In addition, preliminary experiments were carried out in following conditions: catalyst only, visible light only (photolysis), catalyst in the presence of visible light, catalyst in the presence of hydrogen peroxide (Fenton reaction) and visible light in the presence of hydrogen peroxide. For all these conditions, with the exception of the Fenton reaction, no dye degradation was observed. In the case of the Fenton reaction, only 8% of dye decolorization was obtained at 40 min of reaction. Thus, significant dye decolorization and mineralization were only observed for the $ZnFe_2O_4/H_2O_2$/visible light system, as shown in Fig. 4. It is known that the $ZnFe_2O_4$ spinel shows a wide absorption in the visible-light region due to the narrow bandgap (~1.9 eV) [19], which makes it easily excited by visible light, accelerating the degradation of pollutant molecules from aqueous solution. In addition, as previously mentioned, the addition of H_2O_2 into reaction solution generates more $^{\bullet}OH$ radicals, resulting in rapid oxidation of contaminants [39, 40]. E*xplanation* in *details* of the *mechanism* of photo-Fenton catalytic oxidation reaction can be easily found in literature [11, 19, 58-60]. As shown in Fig. 4a, all samples prepared at higher microwave power (1000 W) showed similar and highest catalytic activity, with about 97% decolorization of dye at 40 min of reaction, and about 60% removal

of TOC at 240 min of reaction. This result can be mainly attributed to their similar and highest values of surface areas compared to the samples prepared at smaller microwave power. The apparent rate constants for the dye decolorization and mineralization were estimated by linear regression, as shown in Fig. 4b. They both followed the pseudo first-order kinetics, according to Eqs. (2) and (3):

$$\ln\left(\frac{C}{C_0}\right) = k_d t \quad (2)$$

$$\ln\left(\frac{TOC}{TOC_0}\right) = k_m t \quad (3)$$

where k_d and k_m are the apparent rate constants for the decolorization and mineralization of the dye, respectively, and both were determined from the slope of the respective linear plots.

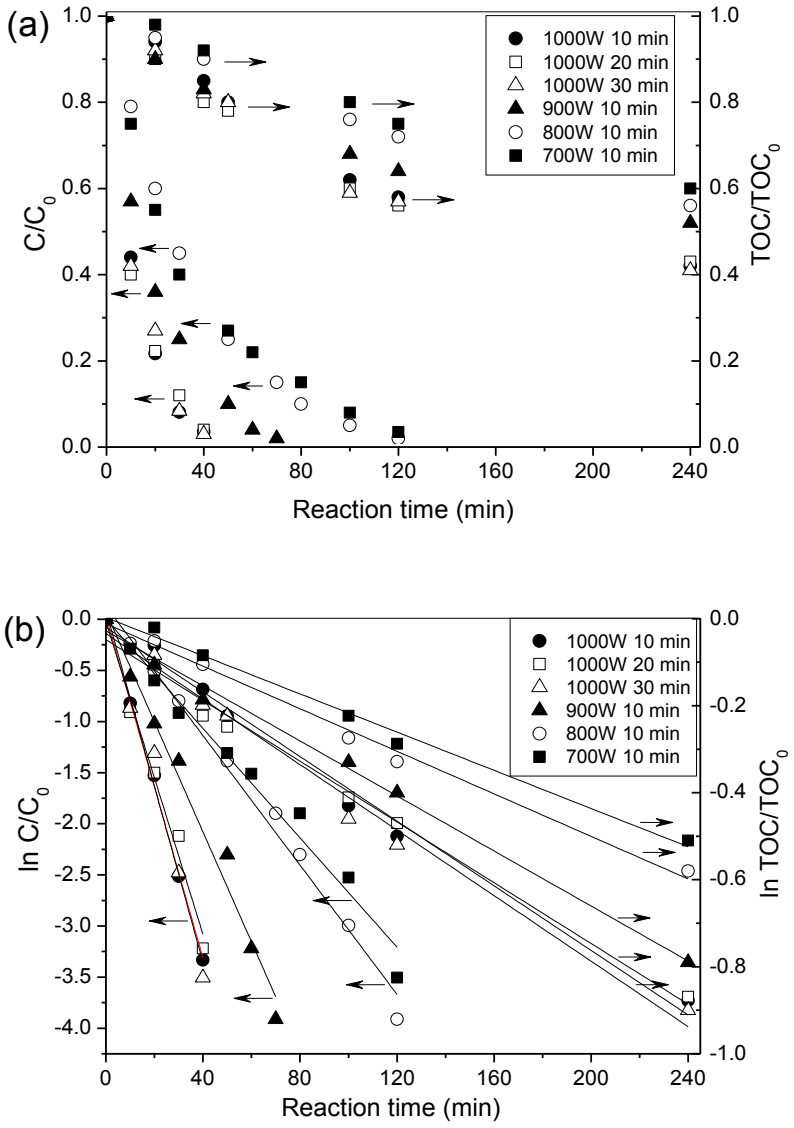

Fig. 4. (a) Decolorization and mineralization profiles of the dye, and (b) variation of ln (C/C_0) and ln (TOC/TOC_0) versus time by photo-Fenton process over $ZnFe_2O_4$ samples.

The decolorization and mineralization rate constants for the Procion Red dye are shown in Table 3. In all the experiments, determination coefficients (R^2) higher than 0.98 were obtained.

Table 3 Apparent rate constants for the dye decolorization and mineralization.

Sample	k_d (min^{-1})	k_m (min^{-1})
1000 W 30 min	86. 22 x 10^{-3}	3.77 x 10^{-3}
1000 W 20 min	78.70 x 10^{-3}	3.49 x 10^{-3}
1000 W 10 min	83.60 x 10^{-3}	3.71 x 10^{-3}
900 W 10 min	53.81 x 10^{-3}	3.16 x 10^{-3}
800 W 10 min	31.65 x 10^{-3}	2.45 x 10^{-3}
700 W 10 min	28.76 x 10^{-3}	2.20 x 10^{-3}

As shown in Table 3, the mineralization rates are much slower than the decolorization rates of dye. These findings have also been observed in other research regarding the pollutant degradation from aqueous solution [58,61,62]. These results indicate that a more extended reaction time is need to the complete mineralization, i.e, complete conversion of the organic pollutant to water, carbon dioxide and other inorganic species. From Table 3, it can be observed that both rate constants (k_d and k_m) of the samples prepared at 1000 W were higher than that of samples prepared in other powers, which can be attributed to their highest surface area values, as above mentioned. The values of the rate constants were similar among the samples prepared at 1000 W due to their similar surface area values, as shown in Table 2. Our recent study [14] has shown that $ZnFe_2O_4$ efficiently degrade Procion Red dye by the photo-Fenton process under visible light. In this study, $ZnFe_2O_4$ particles were prepared by solvothermal conventional method using two diols as solvent, 1,4 butanediol and ethylene glycol. Complete decolorization (k_d = 125 x 10^{-3} min^{-1}) at 30 min and 85% decolorization at 60 min (k_d = 29 x 10^{-3} min^{-1}) were obtained using $ZnFe_2O_4$ samples prepared by 1,4 butanediol and ethylene glycol, respectively. Therefore, the results shown in Table 3 indicate that the $ZnFe_2O_4$ particles indeed exhibit good activity for the degradation of Procion red dye under visible light irradiation.

In order to evaluate the influence of homogeneous photo-Fenton by iron leaching, $ZnFe_2O_4$ particles were removed from the aqueous solution at the end of mineralization (240 min), and an aliquot of H_2O_2 was added into the solution under irradiation. After more 120

min of continuous reaction (without catalyst), no removal of TOC was observed. This indicates that the dye mineralization was induced only by the heterogeneous photo-Fenton reaction on the $ZnFeO_2$ surface. This result is consistent with that of some previous reports which showed that the heterogeneous contribution is dominant for the decolorization/mineralization of the pollutant molecules from aqueous solution [58,62,63]. In addition, within 240 min, practically all added H_2O_2 was decomposed (residual composition of 0.1 mg L^{-1}), indicating a high efficiency of H_2O_2 utilization and a satisfactory degradation and mineralization of the dye in the experimental conditions employed in this work. In all tested samples, the maximum concentration of leached iron at 240 min of irradiation time was 2.7 mg L^{-1}, which is below the level (15 mg L^{-1}) established by the Brazilian environmental legislation (CONAMA) [64] for discharge in waste effluents.

Images in Fig. 5 show $ZnFe_2O_4$ particles prepared at 1000 W for 10 min (Fig. 5a) in suspension and (Fig. 5b) attracted by a magnet, as well as a single particle (Fig. 5c). Fig 5a and 5b were obtained with a digital camera, while Fig 5c was obtained by the AFM technique. Due to their magnetic properties [65,66], $ZnFe_2O_4$ particles can be easily separated and recovered from the aqueous solution by a magnetic field for further reutilization, as shown in Fig. 5b. Fig. 5c displays a single particle of $ZnFe_2O_4$ with irregular morphology and size in sub micrometric scale (around 0.15-0.20 μm).

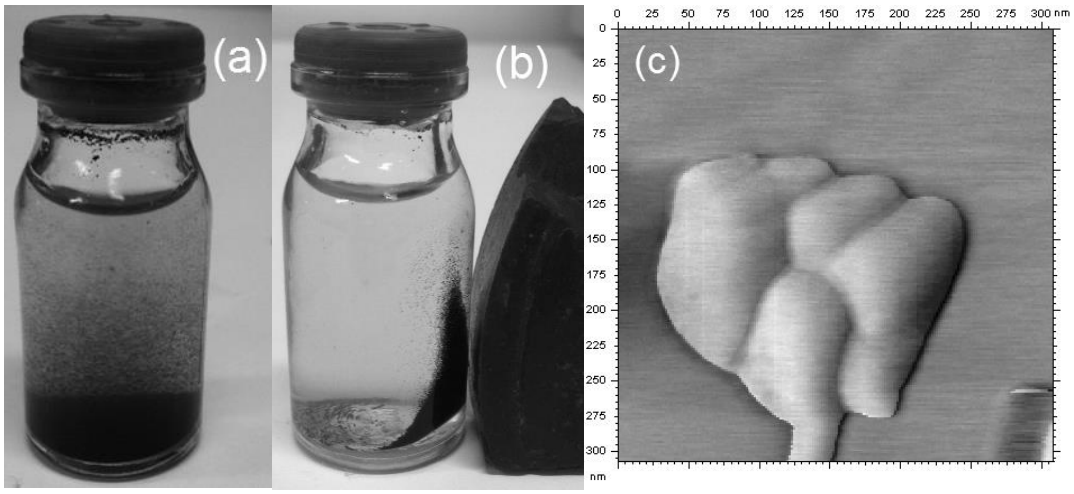

Fig. 5. Photograph of $ZnFe_2O_4$ particles prepared at 1000 W for 10 min (a) in suspension and (b) attracted by a magnet, and (c) AFM image of a single particle.

4. Conclusions

$ZnFe_2O_4$ oxide has been successfully prepared using a rapid and facile synthesis method. The produced material presents high crystallinity and a porous structure, with high surface area. This material was used as a heterogeneous photo-Fenton catalyst which exhibited favorable catalytic activity in degradation of organic pollutants from an aqueous solution in the presence of H_2O_2/visible light. The use of $ZnFe_2O_4$ prepared by microwave technique resulted in nearly 100% of decolorization of dye at 40 min of reaction and 60% of mineralization at 240 min. Therefore, the $ZnFe_2O_4$ catalyst prepared herein shows attractive physical characteristics for the potential application in the field of environmental control for the treatment of emerging organic pollutants.

References

[1] G. Zhang, C. Li, F. Cheng, J. Chen, Sens. Actuators B: Chem. 120 (2007) 403–410.
[2] O.V. Yelenich, S.O. Solopan, T.V. Kolodiazhnyi, V.V. Dzyublyuk, A.I. Tovstolytkin, A.G. Belous, Mater. Chem. Phys. 146 (2014) 129–135.
[3] A. Meidanchi, O. Akhavan, Carbon 69 (2014) 230–238.
[4] F. Tomás-Alonso, J.M.P. Latasa, Fuel Process. Technol. 86 (2004) 191–203.
[5] Z.H. Zhou, J.M. Xue, H.S.O. Chan, J. Wang, Mater. Chem. Phys. 75 (2002) 181–185.
[6] Ž. Cvejić, S. Rakić, S. Jankov, S. Skuban, A. Kapor, J. Alloys Compd. 480 (2009) 241–245.
[7] G. Ma, Y. Chen, L. Li, D. Jiang, R. Qiao, Y. Zhu, Mater. Lett. 131 (2014) 38–41.
[8] H. Lee, J.C. Jung, H. Kim, Y.-M. Chung, T.J. Kim, S.J. Lee, S.-H. Oh, Y.S. Kim, I.K. Song, Catal. Commun. 9 (2008) 1137–1142.
[9] G. Fan, Z. Gu, L. Yang, F. Li, Chem. Eng. J. 155 (2009) 534–541.
[10] L. Liu, G. Zhang, L. Wang, T. Huang, L. Qin, *Ind. Eng. Chem. Res. 50 (*2011) 7219–7227.
[11] M. Su, C. He, V.K. Sharma, M.A. Asi, D. Xia, X. Li, H. Deng, Y._Xiong, J. Hazard. Mater. 211–212 (2012) 95–103.
[12] T. Xie, L. Xu, C. Liu, Y. Wang, Appl. Surf. Sci. 273 (2013) 684–691.
[13] L. Han, X. Zhou, L. Wan, Y. Deng, S. Zhan, J. Environ. Chem. Eng. 2 (2014) 123–130.
[14] C.G. Anchieta, A. Cancelier, M.A. Mazutti, S.L. Jahn, R.C. Kuhn, A. Gündel, O. Chiavone-Filho, E.L. Foletto, Materials 7 (2014) 6281–6290.
[15] X. Huang, J. Zhang, S. Xiao, T. Sang, G. Chen, Mater. Lett. 124 (2014) 126–128.
[16] O. Yalçın, H. Bayrakdar, S. Özüm, J. Magn. Magn. Mater. 343 (2013) 157–162.
[17] H. Liu, Y. Guo, Y. Zhang, F. Wu, Y. Liu, D. Zhang, Mater. Sci. Eng., B 178 (2013) 1057–1061.
[18] J.Y. Patil, D.Y. Nadargi, J.L. Gurav, I.S. Mulla, S.S. Suryavanshi, Ceram. Int. 40 (2014) 10607–10613.
[19] X. Li, Y. Hou, Q. Zhao, L. Wang, J. Coll. Interf. Sci. 358 (2011) 102–108.
[20] C.G. Anchieta, D. Sallet, E.L. Foletto, S.S. Silva, O. Chiavone-Filho, C.A.O. Nascimento, Ceram. Int. 40 (2014) 4173–4178.

[21] A. Sutka, G. Mezinskis, M. Zamovskis, D. Jakovlevs, I. Pavlovska, Ceram. Int. 39 (2013) 8499–8502.
[22] Y. Köseoğlu, A. Baykal, M.S. Toprak, F. Gözüak, A.C. Başaran, B. Aktaş, J. Alloys Compd. 462 (2008) 209–213.
[23] Y. Sun, W. Wang, L. Zhang, S. Sun, E. Gao, Mater. Lett. 98 (2013) 124–127.
[24] Y. Cao, D. Jia, P. Hu, R. Wang, Ceram. Int. 39 (2013) 2989–2994.
[25] Z. Zhao, K. Ouyang, M. Wang, Trans. Nonferrous Met. Soc. China 20 (2010) 1131–1135.
[26] A. Bardhan, C.K. Ghosh, M.K. Mitra, G.C. Das, S. Mukherjee, K.K. Chattopadhyay, Solid State Sci. 12 (2010) 839–844.
[27] R. Dom, R. Subasri, N.Y. Hebalkar, A.S. Chary, P.H. Borse, RSC Adv. 2 (2012) 12782–12791.
[28] A. Manikandan, L.J. Kennedy, M. Bououdina, J.J. Vijaya, J. Magn. Magn. Mater. 349 (2014) 249–258.
[29] S.-W. Cao, Y.-J. Zhu, G.-F. Cheng, Y.-H. Huang, J. Hazard. Mater. 171 (2009) 431–435.
[30] W. Konicki, D. Sibera, E. Mijowska, Z. Lendzion-Bieluń, U. Narkiewicz, J. Coll. Interf. Sci. 398 (2013) 152–160.
[31] V. Blanco-Gutierrez, E. Climent-Pascual, M.J. Torralvo-Fernandez, R. Saez-Puche, M.T. Fernandez-Diaz, J. Solid State Chem. 184 (2011) 1608–1613.
[32] R. Dom, Subasri, R.; Radha, K.; Borse, P. H. *Solid State Commun*. 2011, *151*, 470–473.
[33] M. Kooti, A.N. Sedeh, Scientia Iranica F 19 (2012), 930–933.
[34] E.L. Foletto, J.M. Simões, M.A. Mazutti, S.L. Jahn, E.I. Muller, L.S.F. Pereira, E.M.M. Flores, Ceram. Int. 39 (2013) 4569–4574.
[35] E.L. Foletto, D.S. Paz, A. Gündel, Appl. Clay Sci. 83–84 (2013) 63–67.
[36] B.D. Cullity, S.R. Stock, Elements of X-Ray Diffraction, 3rd Ed., Prentice-Hall Inc., New Jersey, 2001.
[37] E.L. Foletto, C.T. Weber, D.A. Bertuol, M.A. Mazutti, Sep. Sci. Technol. 48 (2013) 2817–2824.
[38] Y. Gao, H. Gan, G. Zhang, Y. Guo, Chem. Eng. J. 217 (2013) 221–230.
[39] A. Babuponnusami, K. Muthukumar, J. Environ. Chem. Eng. 2 (2014) 557–572.
[40] S.-J. Yuan, X.-H. Dai, Appl. Catal. B: Environ. 154–155 (2014) 252–258.
[41] K.S.W. Sing, D.H. Everet, R.A.W. Haul, L. Moscou, R.A. Pieroti, J. Rouquerol, Pure Appl. Chem. 57 (1985) 603—619.
[42] C. Luadthong, V. Itthibenchapong, N. Viriya-empikul , K. Faungnawakij, P. Pavasant, W. Tanthapanichakoon, Mat. Chem. Phys. 143 (2013) 203–208.
[43] N. Kislov, S.S. Srinivasan, Yu. Emirov, E.K. Stefanakos, Mat. Sci. Eng. B 153 (2008) 70–77.
[44] N.-S. Chen, X.-J. Yang, E.-S. Liu, J.-L. Huang, Sens. Actuators B 66 (2000) 178–180.
[45] R. Tholkappiyan, K. Vishista, Int. J. ChemTech Res. 6 (2014) 2834–2842.
[46] S. Khorrami, F. Gharib, G. Mahmoudzadeh, S. Sadat Sepehr, S. Sadat Madani, N. Naderfar, S. Manie, Int. J. Nano. Dim. 1(2011) 221–224.
[47] W. Kim, F. Saito, Powder Techn. 114 (2001) 12–16.
[48] Y. Hou, X. Li, Q. Zhao, G. Chen, Appl. Catal. B: Environ. 142–143 (2013) 80–88.
[49] L. Zhang, Y. He, P. Ye, Y. Wu, T. Wu, J. Alloys Compd. 549 (2013) 105–113.
[50] M. Mouallem-Bahout, S. Bertrand, O. Peña, J. Solid State Chem. 178 (2005) 1080–1086.
[51] N. Rezlescu, E. Rezlescu, F. Tudorache, P.D. Popa, Rom. Rep. Phys. 61 (2009) 223–234.
[52] A. Sutka, G. Mezinskis, A. Pludons, S. Lagzdina, Energetika 3–4 (2010) 254–259.
[53] N. Rezlescu, E. Rezlescu, P.D. Popa, C. Doroftei, M. Ignat, Rom. Rep. Phys. 65 (2013) 1348–1356.

[54] J.S. Jang, P.H. Borse, J.S. Lee, O.-S. Jung, C.-R. Cho, E.D. Jeong, M.G. Ha, M.S. Won, H.G. Kim, Bull. Korean Chem. Soc. 30 (2009), 1738–1742.
[55] R.D. Waldron, Infrared Spectra of Ferrites, Phys. Rev. 99 (1955) 1727–1735.
[56] M.A. Ahmed, E. Ateia, S.I. El-dek, Vibrat. Spectrosc. 30, (2002) 69–75.
[57] J.P. Singh, G. Dixit, R.C. Srivastava, H.M. Agrawal, R. Kumar, J. Alloys Compd. 551 (2013) 370–375.
[58] S. Guo, G. Zhang, J. Wang, J. Coll. Interf. Sci. 433 (2014) 1–8.
[59] S.R. Pouran, A.A.A. Raman, W.M.A.W. Daud, J. Cleaner Prod. 64 (2014) 24–35.
[60] C. Orbeci, I. Untea, G.e Nechifor, A.E. Segneanu, M.E. Craciun, Sep. Purif. Technol. 122 (2014) 290–296.
[61] R.G. Flores, S.L.F. Andersen, L.K.K. Maia, H.J. José, R.F.P.M. Moreira, J. Environ. Manage. 111 (2012) 53–60.
[62] Y. Wang, H. Zhao, M. Li, J. Fan, G. Zhao, Appl. Catal. B: Environ. 147 (2014) 534–545.
[63] X. Zhang, Y. Ding, H. Tang, X. Han, L. Zhu, N. Wang, Chem. Eng. J. 236 (2014) 251–262.
[64] National Council on Environmental (Brazil). Available online: http://www.mma.gov.br/port/conama (accessed on 22 september 2014).
[65] A. Pradeep, P. Priyadharsini, G. Chandrasekaran, J. Alloys Compd. 509 (2011) 3917–3923.
[66] R.P. Patil, S.D. Delekar, D.R. Mane, P.P. Hankare, Results Phys. 3 (2013) 129–133.

3.3 Artigo III: Statistical optimization of Procion Red removal by heterogeneous photo-Fenton reaction using $ZnFe_2O_4$ oxide prepared by microwave irradiation

Chayene Gonçalves Anchieta[1], Guilherme Luiz Dotto[1], Marcio Antonio Mazutti[1], Raquel Cristine Kuhn[1], Gabriela Carvalho Collazzo[1], Osvaldo Chiavone-Filho[2], Edson Luiz Foletto[1]

[1] Departamento de Engenharia Química, Universidade Federal de Santa Maria, 97105-900, Santa Maria, Brasil
[2] Departamento de Engenharia Química, Universidade Federal do Rio Grande do Norte, 59072-970, Natal, Brasil

Artigo a ser submetido a um periódico na área de Engenharias II.

ABSTRACT. A statistical optimization of Procion Red (PR) removal by heterogeneous photo–Fenton reaction using $ZnFe_2O_4$ particles was performed. $ZnFe_2O_4$ oxide was synthesized by microwave-assisted solvothermal route, and characterized by X–ray diffraction, Fourier transform infrared spectroscopy and N_2 adsorption isotherms. This material was used as catalyst for the removal of PR dye from aqueous media. The statistical optimization of PR removal was performed using a 2^{4-1} fractional design, followed by the response surface methodology (RSM), being evaluated the effects of pH, reaction time, dye concentration and H_2O_2 concentration. $ZnFe_2O_4$ particles presented a mesoporous structure with surface area of 65 $m^2\ g^{-1}$. It was found that the more adequate conditions for PR removal were pH 2.0, reaction time of 60 min, dye concentration of 60 mg L^{-1} and H_2O_2 concentration of 10 mM. Under these conditions, the color removal attained about 90%. These results demonstrate that $ZnFe_2O_4$ is an efficient catalyst for the removal PR dye from aqueous media through the photo–Fenton reaction.

Keywords: central composite design, photo–Fenton, dye, statistical optimization, $ZnFe_2O_4$

1. Introduction

Dye-containing effluents from the textile industries can cause various environmental impacts, since contains suspended solids, higher values of oxygen chemical demand, dyes and other soluble substances [1]. Particularly, dye molecules are difficult to be removed from the effluents, because are characterized by high chemical stability and low degradability. It is recognized that the advanced oxidation processes (AOPs) are an emerging technology to remove dyes from aqueous effluents [2].

Among the AOPs, heterogeneous Fenton reaction is one of the most promising technologies remove organic compounds [3-6].

For the case of this technique, due to their magnetic properties [7], *iron-based materials* can be separated and recovered from the aqueous solution by a magnetic field for further reutilization. Several *iron-based materials* such as $FeVO_4$, $CuFe_2O_4$, Fe_3O_4, α–Fe_2O_3 and α–FeOOH have been applied as catalysts in Fenton reaction, in order to remove pollutant compounds [8-11]. According to Pouran et al. [9], several Fe oxides with spinel structure presents high catalytic activity in Fenton reactions. Recently $ZnFe_2O_4$ has gained attention due its high catalytic potential [12-14].

According to Zhang et al. [11] and Guedes et al. [15], to obtain satisfactory results in the effluents treatment using Fenton reaction, different process conditions should be studied. For example, pH, H_2O_2 concentration, reaction time and dye concentration are fundamental factors [15-17]. To decrease the operational costs, these variables should be optimized. The classical methods to evaluate the factors affecting photo–Fenton reaction require many experiments and no taking into account the interaction effects. In this context, response surface methodology (RSM) is an alternative way. RSM minimize the number of experiments and taking into account the interaction effects. Also, statistical models to represent the desired response as a function of the studied variables can be generated [18-23].

In this work, $ZnFe_2O_4$ oxide was used as catalyst in the photo–Fenton reaction to remove Procion Red (PR) from aqueous solution. The $ZnFe_2O_4$ catalyst was synthesized by microwave-assisted solvothermal method and characterized by different techniques. The effects of pH (1.16–4.00), reaction time (10.0–76.8 min), dye concentration (40.0–76.8 mg L^{-1}) and H_2O_2 concentration (20.0–60.0 mM) were evaluated in order to optimize the PR removal by heterogeneous photo–Fenton reaction. The statistical optimization was performed using a 2^{4-1} fractional design, followed by the response surface methodology (RSM).

2. Experimental

2.1. Materials and reagents

The following analytical grade reagents were provided from Synth (Brazil) and Vetec (Brazil): sulfuric acid (H_2SO_4), sodium hydroxide (NaOH), hydrogen peroxide (H_2O_2), zinc nitrate ($Zn(NO_3)_2.6H_2O$), iron nitrate ($Fe(NO_3)_3.9H_2O$), ethyleneglycol ($C_2H_4(OH)_2$) and sodium acetate (CH_3COONa). Procion Red HE–7B dye (PR) (industrial grade, CAS number 61931–52–0; $C_{52}H_{34}O_{26}S_8Cl_{12}N_{14}$, 1952 g mol^{-1}) was provided by a textile company from Brazil southern. This dye was selected because is largely employed in textile industries and is a common pollutant in textile effluents [24, 25].

2.2. Synthesis and characterization of $ZnFe_2O_4$ oxide

$ZnFe_2O_4$ particles were synthesized by microwave-assisted solvothermal route, which was developed in our laboratory. $Zn(NO_3)_2.6H_2O$ and $Fe(NO_3)_3.9H_2O$ were used as precursor salts and ethyleneglycol was used as solvent. The stoichiometric ratio Zn:Fe was 1:2. In brief, 4.0 mmol of $Zn(NO_3)_2.6H_2O$ and 8.0 mmol of $Fe(NO_3)_3.9H_2O$ were dissolved in 120 mL of ethyleneglycol under constant agitation, being added 60.0 mmol of CH_3COONa. After, the solution was transferred to a Teflon reactor and submitted to microwave irradiation (MARS 6 Microwave, ESP 1500 plus, USA) under the following conditions: temperature of 230 °C, power of 600 W and time of 30 min. Finally, the precipitate was removed, washed several times with deionized water and oven dried at 70 °C for 24 h. All the procedures and conditions were developed and defined in our laboratory, on the basis in preliminary tests.

The $ZnFe_2O_4$ catalyst was characterized by X–ray diffraction (XRD), Fourier transform infrared spectroscopy (FTIR) and N_2 adsorption isotherms (BET). The diffractogram of $ZnFe_2O_4$ oxide was obtained in a diffractometer (Rigaku, Miniflex 300, Japan) equipped with Ni–filtered Cu-Kα radiation (λ = 1.54051 Å), with 2θ = 25–65°. The diffractometer was operated with 0.03° diverging and receiving slits at 30 kV and 10 mA. The crystallite mean size (D, Å) was determined by Scherrer equation (Eq. (1)) [26]:

$$D = \frac{K\lambda}{h_{1/2}\cos\theta} \quad (1)$$

Where: K is the Scherrer constant (0.90), $h_{1/2}$ is the width at half height of the more intense peak and θ is the position of this peak (in this work, 2θ= 35.36°). The FTIR spectrum was

obtained using the technique of diffuse reflectance in potassium bromide (Shimadzu, Prestige 21, Japan) [27]. The KBr pellets were prepared with 10 mg of $ZnFe_2O_4$ and 300 mg of KBr. The wavenumber ranged from 4000 to 375 cm^{-1}. The BET surface area and pore size distribution of $ZnFe_2O_4$ catalyst were obtained by N_2 adsorption–desorption isotherms at 77 K with P/P_0 ranging from 0.00 to 0.99 (Micromeritcs, ASAP 2020, USA) [28].

2.3. Photo–Fenton assays

Photo–Fenton assays were performed in a 100 mL batch glass reactor (internal diameter of 5 cm and height of 6 cm) equipped with an economic lamp (Philips, 80 W, 65 lumens W^{-1}). The distance between the liquid surface and the lamp was 15 cm. The PR dye solutions (50 mL), with different initial concentrations (according to the statistical optimization), had the pH adjusted (according to the statistical optimization) and 0.025 g of $ZnFe_2O_4$ were added. The solutions were stirred in the dark, at 100 rpm and 25 °C, until the adsorption equilibrium. After, H_2O_2 was added (according to the statistical optimization) and the irradiation was performed. Samples were collected in preset time intervals (according to the statistical optimization), filtered and the absorbance was determined at a maximum wavelength of 543 nm (Shimadzu–UV1800, Japan). The removal efficiency (*E*, %) was determined as a function of color removal, according to Eq. (2):

$$E = \frac{(A_0 - A)}{A_0} 100 \quad (2)$$

Where: A_0 is the initial absorbance and A is the final absorbance.

2.4. Statistical optimization

The statistical optimization of PR removal by heterogeneous photo–Fenton reaction was performed using a 2^{4-1} fractional design, followed by the response surface methodology (RSM), being evaluated the effects of pH, reaction time, dye concentration and H_2O_2 concentration.

Firstly, a 2^{4-1} fractional design was used in order to verify the individual effects of pH (2.00 and 4.00), reaction time (10.0 and 60.0 min), dye concentration (40.0 and 60.0 mg L^{-1}) and H_2O_2 concentration (20.0 and 60.0 mM). These levels and factors were determined by preliminary tests and shown in literature [1, 10, 11, 17, 29-31]. The real and coded values of the variables are presented in Table 1.

After, in order to obtain the optimal reaction conditions, the removal efficiency (*E*) was optimized using a central rotational composite design (2^3 with three central and six axial points) [18, 21, 32, 33]. The effects of reaction time (from 43.2 to 76.8 min), pH (from 1.16 to 2.84) and dye concentration (from 43.2 to 76.8 mg L^{-1}) were evaluated. The real and coded values of the variables are presented in Table 2. The response (*E*) was represented as a function of independent variables, according to a quadratic polynomial equation (Eq. (3)) [18]:

$$E = a + \sum_{i=1}^{n} b_i x_i + \sum_{i=1}^{n} b_{ii} x_i^2 + \sum_{i=1}^{n-1} \sum_{j=i+1}^{n} b_{ij} x_i x_j \quad (3)$$

Where: a is the constant coefficient, b_i are the linear coefficients, b_{ij} are the interaction coefficients, b_{ii} are the quadratic coefficients and x_i, x_j are the coded values of the variables.

The statistical significance of the nonlinear regression was determined by Student's test, the second order model equation was evaluated by Fischer's test and the proportion of variance explained by the model obtained was given by the coefficient of determination, R^2 [18]. Experimental runs were performed at random and the results were analyzed using Statistic version 9.1 (Statsoft, USA) software.

3. Results and discussion

3.1. Characterization of $ZnFe_2O_4$ oxide

Fig. 1 shows the X–ray diffractogram (a) and FTIR spectrum (b) of $ZnFe_2O_4$ oxide prepared in this work by microwave-assisted solvothermal method.

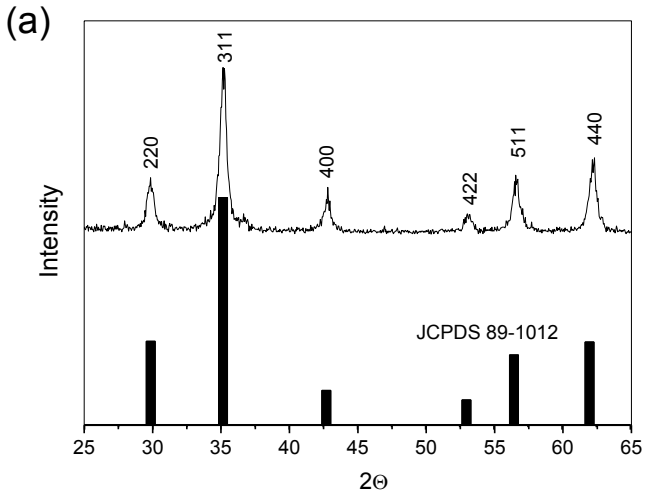

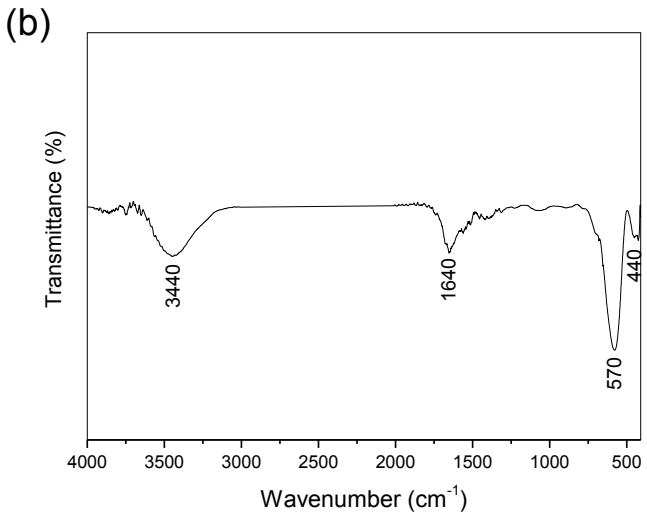

Fig. 1X–ray diffractogram (a) and FTIR spectrum (b) of $ZnFe_2O_4$ oxide.

The X–ray diffractogram (Fig. 1a) shows that $ZnFe_2O_4$ oxide presented a cubic and single phase structure, according to the Joint Committee on Powder Diffraction Standards (JCPDS), card no. 89–1012. The diffraction peaks at 2θ of 30.05°, 35.36°, 42.78°, 52.96°, 56.78° and 62.20° can be attributed to the diffraction planes of (220), (311), (400), (422), (511) and (440), respectively. No impurity was detected. The crystallite mean size (*D*), determined by the Scherrer equation (Eq. 1) was 177 Å. The FTIR spectrum of $ZnFe_2O_4$ (Fig. 1b) shows bands at 3440, 1640, 570 and 440 cm^{-1}. The bands at 3440 and 1640 cm^{-1} can be assigned to the vibration of water molecules on the $ZnFe_2O_4$ surface. The bands, which prove the spinel formation, could be visualized at 570 cm^{-1} (Zn–O) and 440 cm^{-1} (Fe–O) [34, 35].

Fig. 2 shows the N_2 adsorption–desorption isotherms (a) and the pore size distribution (b) of $ZnFe_2O_4$.

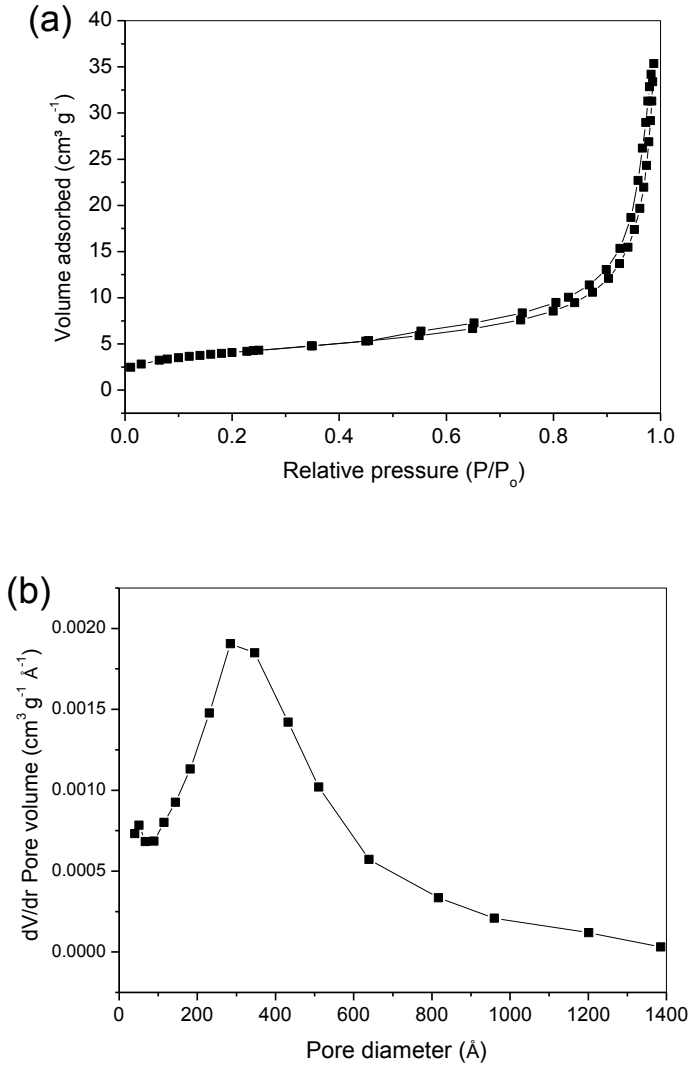

Fig. 2. N_2 adsorption–desorption isotherms (a) and pore size distribution (b) of $ZnFe_2O_4$ oxide.

As can be seen from Fig. 2a, the N_2 adsorption–desorption isotherms are type III curves with H_3 hysteresis, indicating non uniform pores, which were formed by particle agglomerates [36]. The pore size distribution curve (Fig. 2b) indicates a mesoporous structure (20 Å < pore size < 500 Å). This characteristic can be attributed to the voids among agglomerate particles. The $ZnFe_2O_4$ surface area was 65 m^2 g^{-1}, the total pore volume was 0.301 cm^3 g^{-1} and the pore size was 170 Å.

3.2.Fractional design results

PR dye was removed from aqueous solutions by the photo–Fenton reaction using $ZnFe_2O_4$ as catalyst. In order to evaluate the individual effects of pH, reaction time (*t*), dye concentration (*[Dye]*) and H_2O_2 concentration (*[H_2O_2]*) on the PR removal efficiency (*E*), a 2^{4-1} fractional design was employed. The results are shown in Table 1.

Table 1

Experimental conditions (coded and real values) and results for the 2^{4-1} fractional design

Exp.	*[H_2O_2]*/(mM)	*[Dye]*/(mg L^{-1})	*pH*	*t*/(min)	$E_{exp.}$/(%)*	$E_{rep.}$/(%)*
1	1 (60.0)	1 (60.0)	1 (4.00)	1 (60.0)	1.93	2.03
2	1 (60.0)	1 (60.0)	–1 (2.00)	–1 (10.0)	50.39	50.98
3	1 (60.0)	–1 (40.0)	1 (4.00)	–1 (10.0)	0.55	0.62
4	1 (60.0)	–1 (40.0)	–1 (2.00)	1 (60.0)	75.00	74.06
5	–1 (20.0)	1 (60.0)	1 (4.00)	–1 (10.0)	2.20	1.90
6	–1 (20.0)	1 (60.0)	–1 (2.00)	1 (60.0)	90.62	89.04
7	–1 (20.0)	–1 (40.0)	1 (4.00)	1 (60.0)	1.45	1.50
8	–1 (20.0)	–1 (40.0)	–1 (2.00)	–1 (10.0)	47.50	52.05

* *Eexp* = removal efficiency of the experiment and *Erep* = removal efficiency of its replicate. The real values are in brackets.

Based on the results presented in Table 1, the Pareto Chart was constructed to verify the effects of the independent variables on the PR removal efficiency. The Pareto Chart is presented in Fig. 3. It was found in Fig. 3 that all independent variables were significant ($p<0.05$) in relation to the removal efficiency. The pH was the most influent factor, followed by reaction time, dye concentration and H_2O_2 concentration. An inversely proportional dependence of the removal efficiency in relation to the pH, dye concentration and H_2O_2 concentration was observed. The reaction time effect was directly proportional.

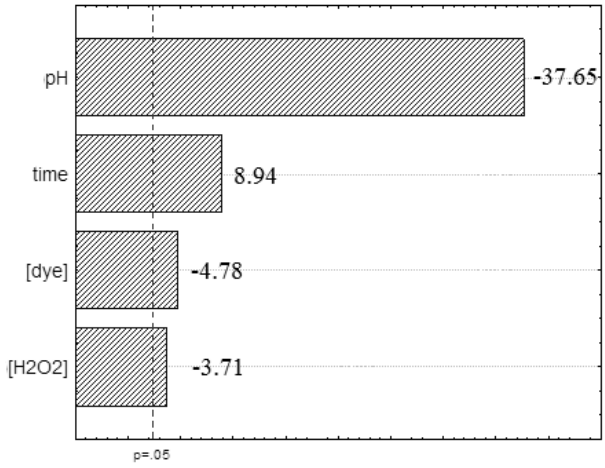

Fig. 3 Pareto Chart for the removal efficiency as a function of the independent variables (fractional design).

The pH was the most influent factor regarding to the PR removal efficiency (Fig. 3), being that, the pH decrease favored the removal efficiency. This behavior is usual in the Fenton reaction. The Fenton technology applies the combination of H_2O_2 and Fe^{2+} in an acidic aqueous medium (pH≤3), producing hydroxyl reactive radicals ($OH^{\bullet}$), which are effective in the oxidation of pollutant molecules [37, 38]. The PR removal efficiency was also favored by the contact time increase and dye concentration decrease (Fig. 2). The H_2O_2 concentration decrease caused an increase in the removal efficiency. This occurred because at higher H_2O_2 concentrations, the $OH^{\bullet}$ radical can be eliminated due to the generation of hydroxyperoxide radicals ($OH_2^{\bullet}$), which is less reactive [38, 39].

The results of a 2^{4-1} fractional design were used to define the levels and factors of central rotational composite design, which was used to optimize the PR removal. Since that pH, reaction time and dye concentration were the most influent factors, they were selected for the central rotational composite design. The central point was pH of 2.00, reaction time of 60.0 min, and 60.0 mg L^{-1} of dye concentration. Once that the H_2O_2 concentration presented an inversely proportional dependence regarding to the removal efficiency, the central rotational composite design experiments were made with 20 mM of H_2O_2.

3.3.Optimization of PR removal

To obtain the optimal reaction conditions, the removal efficiency (*E*) was optimized using a central rotational composite design (2^3 with three central and six axial points). The levels, factors and results of the central rotational composite design are shown in Table 2.

Table 2

Experimental conditions (coded and real values) and results for the 2^3 central rotational composite design

Exp.	*pH*	*[Dye]*/(mg L^{-1})	*t*/(min)	$E_{exp.}$/(%)*
1	1 (2.50)	1 (70.0)	1 (70.0)	47.26
2	1 (2.50)	1 (70.0)	–1 (50.0)	37.50
3	1 (2.50)	–1 (50.0)	1 (70.0)	70.01
4	1 (2.50)	–1 (50.0)	–1 (50.0)	51.32
5	–1 (1.50)	1 (70.0)	1 (70.0)	79.31
6	–1 (1.50)	1 (70.0)	–1 (50.0)	75.57
7	–1 (1.50)	–1 (50.0)	1 (70.0)	71.83
8	–1 (1.50)	–1 (50.0)	–1 (50.0)	32.50
9	–1.68 (1.16)	0 (60.0)	0 (60.0)	56.98
10	1.68 (2.84)	0 (60.0)	0 (60.0)	50.98
11	0 (2.00)	–1.68 (43.2)	0 (60.0)	49.68
12	0 (2.00)	1.68 (76.8)	0 (60.0)	24.53
13	0 (2.00)	0 (60.0)	–1.68 (43.2)	54.11
14	0 (2.00)	0 (60.0)	1.68 (76.8)	79.22
15	0 (2.00)	0 (60.0)	0 (60.0)	89.00
16	0 (2.00)	0 (60.0)	0 (60.0)	90.00
17	0 (2.00)	0 (60.0)	0 (60.0)	89.50

* *Eexp*=removal efficiency of the experiment.

To verify the significance of pH, reaction time and dye concentration in relation to the PR removal efficiency, Pareto chart was used. Pareto chart is presented in Fig. 4.

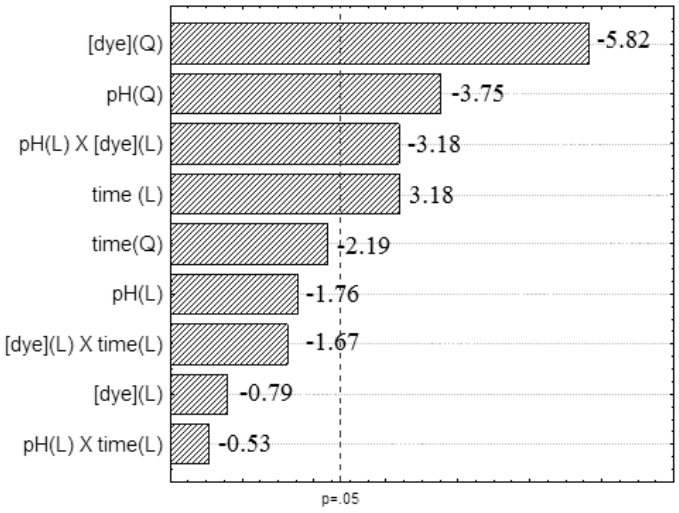

Fig. 4 Pareto Chart for the removal efficiency as a function of the independent variables (central rotational composite design).

It was found in Fig. 4 that the quadratic effects of dye concentration and pH were significant regarding the PR removal efficiency ($p < 0.05$). Also, the interaction effect pH versus dye concentration and the linear effect of reaction time were significant ($p < 0.05$). All other effects were not significant and were removed from the analysis. Based on the Table 2 results, a statistical polynomial quadratic model was proposed to represent the removal efficiency (E) as a function of the significant variables. This empirical model is presented in Eq. (4):

$$E = 89.7 - 10.82\,pH^2 - 16.79\,[Dye]^2 + 8.33t - 10.89\,[Dye]pH \quad (4)$$

For an adequate representation of the experimental data, the statistical model (Eq. (4)) should be significant and predictive [21]. The significance and prediction of the model were evaluated by analysis of variance (ANOVA) and Fischer F test. The determination coefficient was 0.91, showing that the model was significant. The calculated F value ($F_{calc} = 23.4$) was 7.8 times higher than the standard F value ($F_{std} = 3.0$) showing that the model was predictive. The model reliability was also evaluated by the predicted versus observed values (Fig. 5). Fig. 5 shows that the experimental data followed the model tendency.

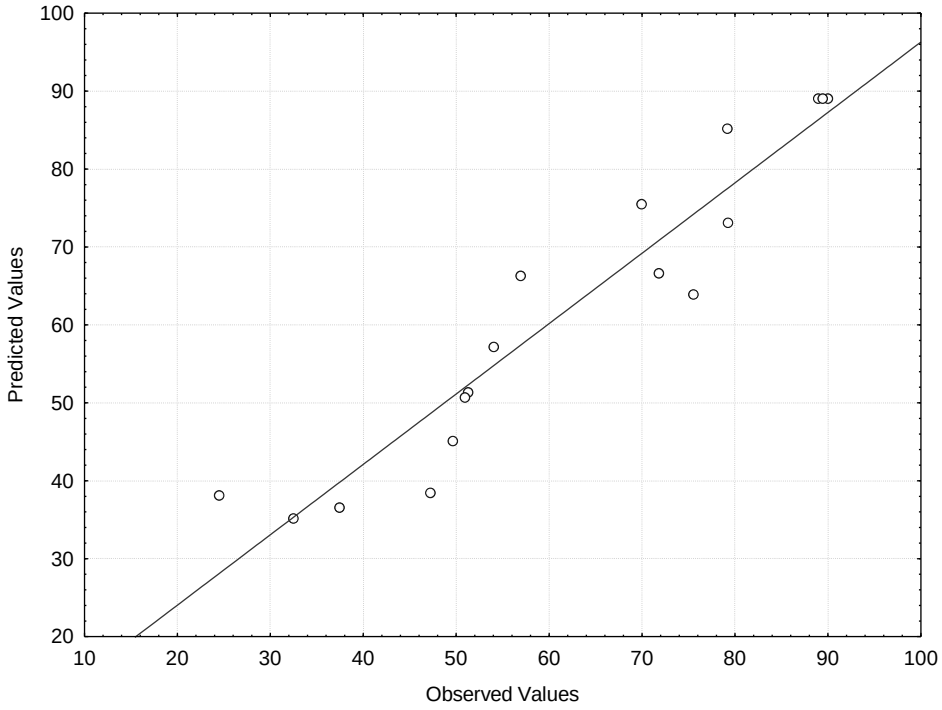

Fig. 5. Predicted *versus* observed values for the removal efficiency.

Once the model is adequate from the statistical viewpoint, the Eq. (4) was used to generate a response surface, which represents the PR removal efficiency as a function of the independent variables. The response surface is presented in Fig. 6.

As can be seen in Fig. 6, the response surface is presented as a function of pH and dye concentration. It can be visualized in Fig. 6 that the PR percentage removal presented a parabolic behavior in relation to the pH and dye concentration, being that the maximum values were attained at the central point. Thus, the optimal conditions for PR removal from aqueous solutions were at pH of 2.00, dye concentration of 60.0 mg L^{-1} and reaction time of 60 min. Under these conditions the removal efficiency was about 90%. Similar values of removal efficiencies of pollutants using heterogeneous Fenton reaction were found by other authors [8, 11, 14]. Therefore the results herein obtained were highly satisfactory and can be attributed to mesoporous structure of $ZnFe_2O_4$ particles.

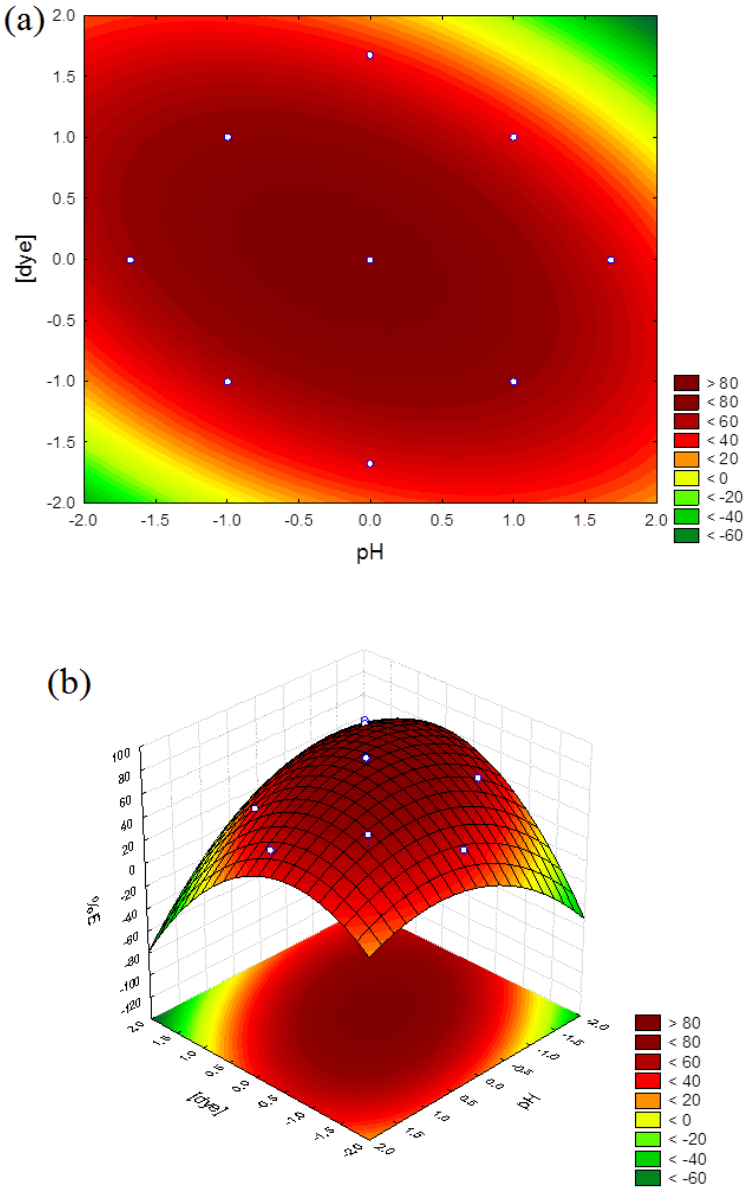

Fig. 6. Contour surface (a) and response surface (b) for the removal efficiency as a function of the independent variables.

4. Conclusions

This work demonstrates that the $ZnFe_2O_4$ catalyst can be successfully synthesized by the microwave-assisted solvothermal route under the following conditions: temperature of 230 °C, power of 600 W and time of 30 min. $ZnFe_2O_4$ spinel presented a mesoporous structure with satisfactory catalytic activity for Procion Red dye degradation. From the statistical optimization, it was possible to provide a significant and predictive model to represent the PR removal efficiency as a function of the independent variables. This model was suitable to predict the PR removal efficiency under the considered experimental conditions. About of

90% of PR removal was attained at pH of 2.00, dye concentration of 60.0 mg L^{-1} and reaction time of 60 min. These results demonstrate that the photo–Fenton reaction using $ZnFe_2O_4$ as catalyst is an adequate technology to remove the PR dye from aqueous solutions.

Acknowledgements

The authors would like to thank CAPES (Coordination for the Improvement of Higher Education Personnel) and CNPq (National Council for Scientific and Technological Development) for the financial support.

References

[1] R. Ansari and Z. Mosayebzadeh, Application of polyaniline as an efficient and novel adsorbent for azo dyes removal from textile wastewaters, Chem. Papers, 65 (2011) 1–8.

[2] P. Oancea and V. Meltzer, Kinetics of tartrazine photodegradation by UV/H_2O_2 in aqueous solution, Chem. Papers, 68 (2014) 105–111.

[3] L. Djeffal, S. Abderrahmane, M. Benzina and S. Siffert, Efficiency of natural clay as heterogeneous Fenton and photo-Fenton catalyst for phenol and tyrosol degradation, Desal. Wat. Treat., 52 (2014) 2225-2230.

[4] Q. Wang, S. Tian, J. Cun and P. Ning, Degradation of methylene blue using a heterogeneous Fenton process catalyzed by ferrocene, Desal. Wat. Treat., 51 (2013), 5821-5830.

[5] Y. Aşçı, Decolorization of Direct Orange 26 by heterogeneous Fenton oxidation, Desal. Wat. Treat., 51 (2013) 7612-7620.

[6] S. Yue, F. Qiyan and L. Xiangdong, Application of response surface methodology to optimize degradation of polyacrylamide in aqueous solution using heterogeneous Fenton process, Desal. Wat. Treat., 53 (20150) 1923-1932.

[7] C. Yao, Q. Zeng, G.F. Goya, T. Torres, J. Liu, H. Wu, M. Ge, Y. Zeng, Y. Wang and J.Z. Jiang, $ZnFe_2O_4$ nanocrystals: synthesis and magnetic properties, *J. Phys. Chem. C*, 111 (2007) 12274–12278.

[8] K. Hanna, T. Kone and G. Medjahdi, Synthesis of the mixed oxides of iron and quartz and their catalytic activities for the Fenton-like oxidation, Catal. Commun., 9 (2008) 955–959.

[9] S.R. Pouran, A.A.A. Raman and W.M.A.W. Daud, Review on the application of modified iron oxides as heterogeneous catalysts in Fenton reactions, J. Cleaner Production, 64 (2014) 24–35.

[10] Y. Wang, H. Zhao, M. Li, J. Fan and G. Zhao, Magnetic ordered mesoporous copper ferrite as a heterogeneous Fenton catalyst for the degradation of imidacloprid. Appl. Catal. B: Environ., 147 (2014) 534–545.

[11] X. Zhang, Y. Ding, H. Tang, X. Han, L. Zhu and N. Wang, Degradation of bisphenol A by hydrogen peroxide activated with $CuFeO_2$ microparticles as a heterogeneous Fenton-like catalyst: efficiency, stability and mechanism, Chem. Eng. J., 236 (2014) 251–262.

[12] X. Li, Y. Hou, Q. Zhao and L. Wang, A general, one-step and template-free synthesis of sphere-like zinc ferrite nanostructures with enhanced photocatalytic activity for dye degradation, J. Coll. Interf. Sci., 358 (2011) 102–108.

[13] J. Wu, W. Pu, C. Yang, G.M. Zhan and J. Zhang, Removal of benzotriazole by heterogeneous photoelectro-Fenton like process using $ZnFe_2O_4$ nanoparticles as catalyst. J. Environ. Sci., 25 (2013) 801–807.

[14] C.G. Anchieta, A. Cancelier, M.A. Mazutti, S.L. Jahn, R.C. Kuhn, A. Gundel, O. Chiavone-Filho and E.L. Foletto, Effects of solvent diols on the synthesis of $ZnFe_2O_4$ particles and their use as heterogeneous photo-Fenton catalysts, *Materials, 7* (2014) 6281–6290.

[15] A.M.F.M. Guedes, L.M.P. Madeira, R.A.R. Boaventura and C.A.V. Costa, Fenton oxidation of cork cooking wastewater—overall kinetic analysis, Water Res., 37 (2003) 3061–3069.

[16] N.N. Mahamuni and Y.G. Adewuyi, Advanced oxidation processes (AOPs) involving ultrasound for waste water treatment: A review with emphasis on cost estimation, Ultrasonics Sonochem., 17 (2010) 990–1003.

[17] T. Mackuľak, M. Smolinska, P. Olejnikova, J. Prousek and A. Takačova, Reduction of ostazine dyes' photodynamic effect by Fenton reaction, Chem. Papers, 66 (2012) 156–160.

[18] R.H. Myers and D.C. Montgomery, Response surface methodology: process and product optimization using designed experiments, New York, 2nd ed., John Wiley & Sons, 2002.

[19] I. Arslan-Alaton, A.B. Yalabik and T. Olmez-Hanci, Development of experimental design models to predict Photo-Fenton oxidation of a commercially important naphthalene sulfonate and its organic carbon content, Chem. Eng. J., 165 (2010) 597–606.

[20] V. Homem, A. Alves and L. Santos, Amoxicillin degradation at ppb levels by Fenton's oxidation using design of experiments, Sci. Total Environ., 408 (2010) 6272–6280.

[21] G.L. Dotto, V.M. Esquerdo, M.L.G. Vieira and L.A.A. Pinto, Optimization and kinetic analysis of food dyes biosorption by Spirulinaplatensis, Coll. Surf. B: Biointerf., 91 (2012) 234–241.

[22] W. Li, B. Li, W. Ding, J. Wu, C. Zhang and D. Fu, Response surface methodology as a tool to optimize the electrochemical incineration of bromophenol blue on boron-doped diamond anode, Diamond Related Mat., 50 (2014) 1–8.

[23] S. Veloutsou, E. Bizani and K. Fytiano, Photo-Fenton decomposition of β-blockers atenolol and metoprolol; study and optimization of system parameters and identification of intermediates, Chemosphere, 107 (2014) 180–186.

[24] E.L. Foletto, S. Battiston, J.M. Simões, M.M. Bassaco, L.S.F. Pereira, E.M.M. Flores and E.I. Müller, Synthesis of $ZnAl_2O_4$ nanoparticles by different routes and the effect of its pore size on the photocatalytic process, Micropor. Mesopor. Mat., 163 (2012) 29–33.

[25] E.L. Foletto, J.M. Simões, M.A. Mazutti, S.L. Jahn, E.I. Muller, L.S.F. Pereira and E.M.M. Flores, Application of Zn_2SnO_4 photocatalyst prepared by microwave-assisted hydrothermal route in the degradation of organic pollutant under sunlight, Ceramics Inter., 39 (2013) 4569–4574.

[26] B.D. Cullity and S.R. Stock, Elements of X-ray diffraction, New Jersey: 3rd Ed., Prentice-Hall Inc, 2001.

[27] R.M. Silverstein, F.X. Webster and D.J. Kiemle, Spectrometric identification of organic compounds, 7th Ed., New York, J. Wiley & Sons, 2005.

[28] S. Brunauer, P.H. Emmett and E. Teller, Adsorption of gases in multimolecular layers, J. Amer. Chem. Soc., 60 (1938) 3091–318.

[29] L. Lu, Y. Ma, M. Kumar and J.G. Lin, Photo-Fenton pretreatment of carbofuran – Analyses via experimental design, detoxification and biodegradability enhancement, Sep. Purif. Techn., 81 (2011) 325–331.

[30] A.D. Bokare and W. Choi, Review of iron-free Fenton-like systems for activating H_2O_2 in advanced oxidation processes, J. Hazard. Mat., 275 (2014) 121–135.

[31] C. Orbeci, I. Untea, G. Nechifor, A.E. Segneanu and M.E. Craciun, Effect of a modified photo-Fenton procedure on the oxidative degradation of antibiotics in aqueous solutions, Sep. Purif. Techn., 122 (2014) 290–296.

[32] G.L. Dotto and L.A.A. Pinto, Adsorption of food dyes onto chitosan: Optimization process and kinetic, Carbohydrate Polym., 84 (2011) 231–238.

[33] T.V. Rêgo, T.R.S. Cadaval Jr., G.L. Dotto and L.A.A. Pinto, Statistical optimization, interaction analysis and desorption studies for the azo dyes adsorption onto chitosan films, J. Coll. Interf. Sci., 411 (2013) 27–33.

[34] N.M. Mahmoodi, Zinc ferrite nanoparticle as a magnetic catalyst: synthesis and dye degradation, Mat. Res. Bull., 48 (2013) 4255–4260.

[35] C.G. Anchieta, D. Sallet, E.L. Foletto, S.S. Silva, O. Chiavone-Filho and C.A.O. Nascimento, Synthesis of ternary zinc spinel oxides and their application in the photodegradation of organic pollutant, Ceramics Inter., 40 (2014) 4173–4178.

[36] K.S.W. Sing, D.H. Everet, R.A.W. Haul, L. Moscou, R.A. Pieroti, J. Rouquerol and T. Siemieniewska, Reporting physisorption data for gas/solid systems with special reference to the determination of surface area and porosity, Pure Appl. Chem., 57 (1985) 603–619.

[37] R. Andreozzi, V. Caprio, A. Insola, R. Marotta, Advanced oxidation processes (AOP) for water purification and recovery, Catal. Today, 53 (1999) 51–59.
[38] Y. Gao, H. Gan, G. Zhang and Y. Guo, Visible light assisted Fenton-like degradation of rhodamine B and 4-nitrophenol solutions with a stable poly-hydroxyl-iron/sepiolite catalyst, Chem. Eng. J., 217 (2013) 221–230.

[39] A.N. Soon and B.H. Hameed, Degradation of acid blue 29 in visible light radiation using iron modified mesoporous silica as heterogeneous photo-Fenton catalyst. Appl. Catal. A: Gen., 450 (2013) 96–105.

CAPITULO 4

CONCLUSÕES

As rotas de síntese propostas neste trabalho, solvotérmica convencional e solvotérmica assistida por microondas, formaram o espinélio ferrita de zinco com sucesso.

As rotas de síntese bem como a variação dos parâmetros de síntese influenciaram significativamente sobre as propriedades físicas do material produzido.

Com relação à síntese de $ZnFe_2O_4$ pelo método solvotérmico convencional, os resultados comprovam que quando se utiliza etilenoglicol ou 1,4 butanodiol como solventes, diferentes características físicas das partículas tais como área superficial e estrutura de poros são obtidas. Nesse método, tempo mais longos de síntese são necessários para a formação das partículas. Neste caso, partículas de ferrita foram formadas em 24 h. Com relação a atividade catalítica na reação heterogênea de foto-Fenton, a ferrita de zinco sintetizada com 1,4 butanodiol apresentou uma velocidade de degradação do corante bem maior do que aquela com o uso de ferrita produzida pelo uso do etilenoglicol, sendo atribuído a sua maior área superficial.

Com relação à síntese de $ZnFe_2O_4$ pelo método solvotérmico assistido por micro-ondas, condições do processo de síntese como tempo e potência de irradiação de microondas foram investigadas. Ocorreu a formação das partículas de ferrita a partir 10 min de irradiação com uma potencia de 700W, e verificou-se que com o aumento da potência (em 1000 W), independentemente do tempo usado (10, 20 e 30 min), superior área superficial foi obtida. Com isso, as amostras preparadas a 1000 W formam as que apresentaram maior atividade para a degradação do corante orgânico.

Por último, um planejamento fatorial foi desenvolvido a fim de avaliar a influência das variáveis de processo envolvidas na degradação do corante, e com isso, otimizá-las de forma a se obter a máxima degradação possível. Constatou-se que as variáveis tais como tempo, pH e concentração de corante e de peróxido de hidrogênio influenciam sobre a degradação do corante. Além disso, um modelo que descreve a reação de degradação do corante foi obtido, sendo que este modelo predizer o resultado experimental com mais de 90% de precisão.

SUGESTÕES PARA TRABALHOS FUTUROS:

- ✓ Testar ciclo de vida do catalisador e sua desativação nas condições ótimas do processo;
- ✓ Testar o uso de ferrita de zinco como catalisador para reação foto- Fenton para degradação de outros compostos orgânicos;
- ✓ Avaliar a influência da concentração de ferro e zinco e reagentes percursores, nas rotas de síntese, sobre as propriedades do material produzido;
- ✓ Testar novas rotas de síntese diferentes daquelas usadas nesse trabalho.